IEEE Access
Multidisciplinary ⋮ Rapid Review ⋮ Open Access Journal

Received 7 November 2022, accepted 13 December 2022, date of publication 19 December 2022,
date of current version 27 December 2022.

Digital Object Identifier 10.1109/ACCESS.2022.3230650

RESEARCH ARTICLE

A Unified Performance Analysis of Cooperative NOMA With Practical Constraints: Hardware Impairment, Imperfect SIC and CSI

SAFIA BEDDIAF[1], ABDELLATIF KHELIL[1], FAICAL KHENNOUFA[1], FERDI KARA[2,3], (Senior Member, IEEE), HAKAN KAYA[4], XINGWANG LI[5], (Senior Member, IEEE), KHALED RABIE[6], (Senior Member, IEEE), AND HALIM YANIKOMEROGLU[3], (Fellow, IEEE)

[1]LGEERE Laboratory, Department of Electrical Engineering, Echahid Hamma Lakhdar University, El-Oued 39000, Algeria
[2]Department of Computer Engineering, Zonguldak Bulent Ecevit University, 67100 Zonguldak, Türkiye
[3]Department of Systems and Computer Engineering, Carleton University, Ottawa, ON K1S 5B6, Canada
[4]Department of Electrical and Electronics Engineering, Zonguldak Bulent Ecevit University, 67100 Zonguldak, Türkiye
[5]School of Physics and Electronic Information Engineering, Henan Polytechnic University, Jiaozuo 454099, China
[6]Department of Engineering, Manchester Metropolitan University, M1 5GD Manchester, U.K.

Corresponding author: Ferdi Kara (f.kara@beun.edu.tr)

The work of Ferdi Kara was supported by the Scientific and Technological Research Council of Türkiye (TUBITAK).

ABSTRACT Non-orthogonal multiple access (NOMA) has been a strong candidate to support massive connectivity in future wireless networks. In this regard, its implementation into cooperative relaying, named cooperative-NOMA (CNOMA), has received tremendous attention from researchers. However, most of the existing CNOMA studies have failed to address practical constraints since they assume ideal conditions. Particularly, the error performance of CNOMA schemes with imperfections has not been investigated yet. In this paper, we provide an analytical framework for error and outage performance of CNOMA schemes under practical assumptions where we take into account imperfect successive interference canceler (ipSIC), imperfect channel state information (ipCSI), and hardware impairments (HWI) at the transceivers. We derive analytical expressions of bit error rate (BER) expressions in CNOMA schemes whether the direct links between source and users exist or not which is, to the best of the authors' knowledge, the first study in the open literature. We also derive the outage probability (OP) expressions for CNOMA schemes with and without direct links under practical assumptions. For comparisons, we provide BER and OP expressions for downlink NOMA with practical constraints which also have not been given in the literature, yet. The theoretical BER and OP expressions are validated with computer simulations where the perfect match is observed. Finally, we discuss the effects of the system parameters (e.g., power allocation, HWI level, ipCSI factor) on the performance of CNOMA schemes to reveal fruitful insights for society. The results demonstrate that the HWI, ipCSI and ipSIC have a significant effect on the performance of the systems.

INDEX TERMS BER, cooperative NOMA, HWI, imperfections, ipCSI, ipSIC, OP, practical constraints.

I. INTRODUCTION

Non-orthogonal multiple access (NOMA) is a promising solution to satisfy the demands for spectrum efficiency and network density in the next generations of wireless access. Therefore, the integration of the NOMA with cooperative relaying (CNOMA) networks has attracted recent attention to improve transmission reliability and extend network coverage and increase spectral efficiency [1]. In CNOMA schemes, there are two possible configurations depending on whether direct links are available between the source and users or not. In the first, the relay node(s) improves the key performance indicators (KPIs), e.g., capacity, outage probability (OP) and bit error rate (BER), while in the second, the relay node(s)

The associate editor coordinating the review of this manuscript and approving it for publication was Tiankui Zhang.

extends the coverage. Nevertheless, almost all literature is devoted to the second scenario where the direct links (DLs) are blocked by some obstacles. To enhance the outage performance of the users, the authors in [2] presented the CNOMA with the aid of a decode-and-forward (DF) relay with different relaying schemes by using both direct and relaying links. In [3], the impact of the DF selection relay on the performance of CNOMA is analyzed with two types of relay selection in terms of OP over Rayleigh fading channel. The authors in [4] examined the outage performance of the amplify-and-forward (AF) relay CNOMA network over the Rayleigh fading channel. The ergodic sum rate and OP of CNOMA with DF and AF protocols over the Nakagami-m fading channels have been analyzed in [5]. Therefore, to improve the performance of the DF CNOMA system, the hybrid relaying scheme that switches between full and half duplex (FD/HD) has been investigated in [6] and [7]. For a more realistic system, the authors in [8] analyzed the residual self-interference and residual multiple access interferences due to imperfect co-channel interference cancellation on the FD-CNOMA over Nakagami-channel in terms of OP and ergodic capacity. The FD/HD coordinated direct and DF relay transmission in the NOMA system is analyzed in terms of OP and ergodic sum rate under imperfect channel state information (ipCSI) and imperfect successive interference cancellation (ipSIC) in [9]. Additionally, the authors in [10] presented a dual-hop multi-relay NOMA using the DF system over Nakagami-m fading channel in terms of OP. A novel two-stage power allocation (PA) scheme with NOMA was proposed to improve the sum rate and the OP of the dual-hop relay system in [11]. The authors in [12] presented the sum rate analysis of the CNOMA scheme with dual-hop hybrid wireless-power line communication. In [13], the performance of the dual-hop DF relay system using NOMA under the assumption of statistical CSI is evaluated. The authors in [14] studied and compared the performance of dual-hop relaying systems adopting DF and AF forwarding strategies. Moreover, a unified framework of NOMA networks that applied the code-domain (CD) and power-domain (PD) NOMA with ipSIC and perfect SIC in terms of OP and throughput is investigated in [15]. The authors in [16] examined the impact of physical layer secrecy on the performance of a unified NOMA framework, where both external and internal eavesdropping scenarios are evaluated in terms of secrecy OP for both CD-NOMA and PD-NOMA under ipSIC and perfect SIC. In order to model the locations of NOMA users within the networks, a unified downlink NOMA transmission scenario has been investigated in [17].

On the other hand, the radio-frequency (RF) equipment is one of the most significant components of the massive network of interconnected devices that facilitates communication between individual devices and/or their base station (BS). Therefore, the direct conversion transceivers seem to be the RF front-end solution to stringent design goals such as low cost, low power dissipation, improved efficiency and performance [18]. However, in a realistic communication scenario, the RF component suffers from various types of hardware impairment (HWI) that limit the performance of the overall system, such as oscillator phase noise (PN), high power amplifier (HPA) and in-phase and quadrature-phase imbalance (IQI) [19], [20]. The effect of individual HWI on the system's performance has been examined in [21], [22], and [23], where the authors in [21] and [23] analyzed throughput and OP performance with the impacts of IQI on the transceiver front-end of the AF two-hop relay node with different IQI levels. The impact of non-linear HPA has been studied in [22], where the OP, ergodic capacity and BER performance deteriorated compared to linear HPA. In [24], the achievable rate has been examined for the massive multiple-input-multiple-output (MIMO) FD relaying in the presence of HWI. In [25], the effect of HWI on one and two ways AF systems in terms of OP expressions has been performed.

As well as other communication techniques [22], [24], [25] given above, the effects of such imperfections on the performance of CNOMA schemes have been examined in several studies [26], [27], [28], [29], [30], [31], [32]. The performance of NOMA dual-hop AF relaying networks is examined over the Nakagami-m fading channel in terms of OP and ergodic sum rate in [26]. An AF CNOMA system with HWI is analyzed in terms of OP and intercept probability over multipath fading channel in [27]. The impact of HWI is investigated on the NOMA-based AF relaying network in terms of OP, ergodic capacity and ergodic sum rate. The authors in [28] investigate the OP and ergodic rate performance of the FD-CNOMA with the presence of HWI over the Rician fading channels. Furthermore, the effect of the simultaneous wireless information and power transfer NOMA system has been analyzed in terms of OP [29]. However, the CNOMA network suffers also from imperfect successive interference cancellation (ipSIC) and imperfect channel state information (ipCSI). The authors in [30] study the impacts of HWI on the NOMA with ipCSI, where both cooperative and non-cooperative NOMA are analyzed in terms of OP, ergodic capacity and energy efficiency. In [31], the OP of the cognitive radio NOMA network is analyzed under HWI, ipCSI and ipSIC. On the other hand, BER performances of FD-CNOMA have been investigated in [33] with ipSIC where perfect CSI and no HWI are considered. Then, the BER and OP performances of a two-hop and multi-hop DF CNOMA with ipCSI has been investigated in [34], [35], and [36]. The pairwise error probability is derived for the AF-CNOMA by considering HWI with no ipCSI [32]. Besides, the BER of the NOMA arbitrary number of users and modulation orders has been analyzed in [37], [38], and [39], which proved that the increase in number of users or modulations order causes infeasible PA. In those cases, some of the users needs to get very low power coefficients.

All the aforementioned CNOMA studies investigate the performances of CNOMA without DLs (DL) and CNOMA with DL has not been investigated with imperfections in terms of any performance metrics. Besides, most of the above papers [1], [2], [9], [15], [16], [27], [28], [30], [31] analyze

the effects of one or multiple imperfections only in terms of achievable rate and/or OP whilst the BER performance is considered in very limited studies [32], [33], [34], [35].

Furthermore, the effects of HWI on the BER performances of NOMA with/without cooperative relaying have not been studied well although its effects on capacity and OP performances have been evaluated in [27], [28], [30], and [31]. Also, the OP with the effect of HWI on CNOMA when maximum ratio combining (MRC) is implemented at the receiver in the presence of ipSIC and ipCSI has not been performed. As discussed above, to the best of our knowledge, the BER and OP performance of NOMA schemes (with/without cooperative relaying) has not been investigated with practical constraints (i.e., ipSIC, ipCSI and HWI). Besides, the BER performance of NOMA with/without cooperative has not been revealed with all imperfections in the open literature.

Motivated by this, in this paper, we provide a comprehensive analytical framework for the BER and OP performances of NOMA schemes under practical constraints where we consider ipSIC, ipCSI and HWI. Therefore, the main contributions of the paper can be summarized as follows.

- Three different schemes of the NOMA system (downlink NOMA, CNOMA without direct link, CNOMA with direct link) are presented with practical constraints (i.e., ipSIC, ipCSI and HWI).
- The exact BER expressions of the three considered systems are derived under HWI in the presence of ipSIC and ipCSI and the analytical results are validated via computer simulations.
- The outage performance for the different NOMA schemes is also investigated and exact OP expressions are derived under HWI, ipCSI and ipSIC. The asymptotic analysis of OP at high SNR regions is performed to reveal the insights of the parameters for HWI, ipCSI, and ipSIC on system performance and the results show that the OP is affected by HWI, ipCSI and ipSIC in the high SNR. In addition, the computer simulations show a perfect-match with theoretical results.
- For the sake of comparisons, extensive computer simulations are presented to reveal the effects of HWI, ipCSI and ipSIC on the BER and OP performance of the considered systems with different scenarios (e.g., PA, and distance between nodes).
- We consider the conventional OMA schemes as a benchmark for comparison with proposed NOMA schemes. Therefore, we obtain the BER and OP system analysis for our three NOMA schemes in the presence of HWI, ipCSI and ipSIC.

The rest of the paper is organized as follows. The CNOMA schemes with/without DLs are introduced in Section II. In Section III, we analyze the exact end-to-end (e2e) BER and OP expressions. The simulation results are presented in Section IV. Finally, Section V concludes the paper.

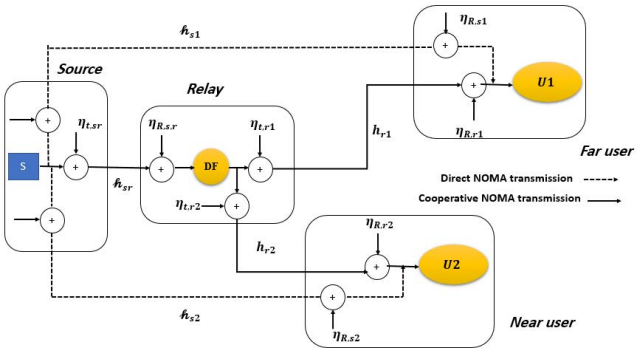

FIGURE 1. System model CNOMA schemes with HWI.

II. SYSTEM MODEL

We consider a downlink CNOMA system as presented in Fig. 1. The model consists of a source (S), a DF relay (R) and two users: user 1 (u1) and user 2 (u2). The S, users and R are equipped with a single antenna and R works in half duplex mode. We assume three different scenarios of the considered system, given as follows.

1) **Downlink NOMA:** S transmits directly the signal to the users, namely, NOMA.
2) **Cooeprative without DL:** S communicates with users with the aid of R without a DL between the S and users, namely, CNOMA.
3) **Cooperative NOMA with DL:** S sends the signal to the users through the R and the DLs, where the users combine both received signals in two phases, namely, CNOMA-WDL.

The communication is completed in a single phase for downlink NOMA whereas it requires two phases in cooperative schemes. The complex flat fading channel coefficient between S-users, R-users and S-R are denoted as $h_{si} \sim \mathcal{CN}(0,\ \sigma_{si}^2)$, $h_{ri} \sim \mathcal{CN}(0,\ \sigma_{ri}^2)$ and $h_{sr} \sim \mathcal{CN}(0,\ \sigma_{sr}^2)$, where $i = 1,\ 2$, respectively. $\sigma_{h_{si}}^2 = d_{h_{si}}^{-a}$, $\sigma_{h_{ri}}^2 = d_{h_{ri}}^{-a}$ and $\sigma_{h_{sr}}^2 = d_{h_{sr}}^{-a}$, where $d_{h_{si}}$, $d_{h_{ri}}$ and $d_{h_{sr}}$ are distances between related nodes and a is the path loss exponent. We assume that the ipCSI exists for each node. The estimated channel coefficients are given as $\tilde{h}_{si} = h_{si} - e$, $\tilde{h}_{ri} = h_{ri} - e$ and $\tilde{h}_{sr} = h_{sr} - e$, where the channel estimation error is presented as $e \sim \mathcal{CN}(0,\ \sigma_\epsilon^2)$. Since $\tilde{h}_{si}, \tilde{h}_{ri}, \tilde{h}_{sr}$ and e are independent, then it can be modeled as $\sigma_{\tilde{h}_{si}}^2 = \sigma_{h_{si}}^2 - \sigma_\epsilon^2$, $\sigma_{\tilde{h}_{ri}}^2 = \sigma_{h_{ri}}^2 - \sigma_\epsilon^2$ and $\sigma_{\tilde{h}_{sr}}^2 = \sigma_{h_{sr}}^2 - \sigma_\epsilon^2$ [40]. As presented in Fig 1, the S transmits a superimposed coding (SC) signal $s_{sc} = \sqrt{\alpha_1} m_1 + \sqrt{\alpha_2} m_2$ to R and users with different PA coefficients according to channel gain $E[|\tilde{h}_{s1}|^2] < E[|\tilde{h}_{s2}|^2]$. The received signals at u1, u2 and R (for cooperative schemes) are given as

$$y_{si} = (\tilde{h}_{si} + e)(\sqrt{P_s} s_{sc} + \eta_{t,si}) + \eta_{R,si} + n_{si}, \quad (1)$$

$$y_{sr} = (\tilde{h}_{sr} + e)(\sqrt{P_s} s_{sc} + \eta_{t,sr}) + \eta_{R,sr} + n_{sr}, \quad (2)$$

where m_1, m_2 are the messages of the u1 and u2, and α_1, α_2 are the PA coefficients of u1 and u2, respectively. In order to improve the fairness in the NOMA system, we suppose that $\alpha_1 > \alpha_2$ and $\alpha_1 + \alpha_2 = 1$. P_s is the transmit power

of S. $\eta_{t,si}$,$\eta_{t,sr}$ and $\eta_{R,si}$,$\eta_{R,sr}$ are distortion noises at the transmitter and receiver, respectively, which occur due to the HWI at transceivers such as PN, HPA and IQI. We assume $n_{si} = n_{sr} = n$ and it is the additive white Gaussian noise (AWGN) which follows $n \sim \mathcal{CN}(0, \frac{N_0}{2})$. The distortion noises are defined as [40]

$$\begin{aligned} &\eta_{t,si} \sim \mathcal{CN}(0,\ k_{t,si}^2 P_s),\ \eta_{R,si} \sim \mathcal{CN}(0,\ k_{R,si}^2 P_s |\tilde{h}_{si}|^2), \\ &\eta_{t,sr} \sim \mathcal{CN}(0,\ k_{t,sr}^2 P_s),\ \eta_{R,sr} \sim \mathcal{CN}(0,\ k_{R,sr}^2 P_s |\tilde{h}_{sr}|^2), \end{aligned} \tag{3}$$

where $k_{t,si}^2$, $k_{t,sr}^2$ and $k_{R,si}^2$, $k_{R,sr}^2$ represent levels of impairment at the transmitter and receiver, respectively. Then, (1) and (2) can be regarded as

$$y_{si} = (\tilde{h}_{si} + e)(\sqrt{P_s} s_{sc} + \eta_{si}) + n, \tag{4}$$
$$y_{sr} = (\tilde{h}_{sr} + e)(\sqrt{P_s} s_{sc} + \eta_{sr}) + n, \tag{5}$$

where η_{si} and η_{sr} are the independent distortion noise terms defined as $\eta_{si} \sim \mathcal{CN}(0,\ k_{si}^2 P_s)$, $\eta_{sr} \sim \mathcal{CN}(0,\ k_{sr}^2 P_s)$, k_{si}^2 and k_{sr}^2 are the HWI level at the transceivers. It has been demonstrated in [40] that the impact of the transceiver HWI can be characterized by the aggregate level of impairments, $k_{si}^2 = k_{t,si}^2 + k_{R,si}^2$ and $k_{sr}^2 = k_{t,sr}^2 + k_{R,sr}^2$.

In the downlink NOMA, the u1, u2 and R decode m_1 message directly by maximum-likelihood detection (MLD). The received signal-to-interference plus noise ratio (SINR) for the m_1 symbol at the u1, u2 and R are given as

$$\gamma_1^{s1} = \frac{\alpha_1 P_s |\tilde{h}_{s1}|^2}{\alpha_2 P_s |\tilde{h}_{s1}|^2 + \sigma_\epsilon^2 P_s + \sigma_\epsilon^2 P_s k_{s1}^2 + |\tilde{h}_{s1}|^2 P_s k_{s1}^2 + \frac{N_0}{2}}, \tag{6}$$

$$\gamma_1^{s2} = \frac{\alpha_1 P_s |\tilde{h}_{s2}|^2}{\alpha_2 P_s |\tilde{h}_{s2}|^2 + \sigma_\epsilon^2 P_s + \sigma_\epsilon^2 P_s k_{s2}^2 + |\tilde{h}_{s2}|^2 P_s k_{s2}^2 + \frac{N_0}{2}}, \tag{7}$$

$$\gamma_1^{sr} = \frac{\alpha_1 P_s |\tilde{h}_{sr}|^2}{\alpha_2 P_s |\tilde{h}_{sr}|^2 + \sigma_\epsilon^2 P_s + \sigma_\epsilon^2 P_s k_{sr}^2 + |\tilde{h}_{sr}|^2 P_s k_{sr}^2 + \frac{N_0}{2}}. \tag{8}$$

However, the u2 and R perform a SIC to detect m_2. The SINR of m_2 at the u2 and R are presented, respectively, as

$$\gamma_2^{s2} = \frac{\alpha_2 P_s |\tilde{h}_{s2}|^2}{\varsigma \alpha_1 P_s |\tilde{h}_{s2}|^2 + \sigma_\epsilon^2 P_s + \sigma_\epsilon^2 P_s k_{s2}^2 + |\tilde{h}_{s2}|^2 P_s k_{s2}^2 + \frac{N_0}{2}}, \tag{9}$$

$$\gamma_2^{sr} = \frac{\alpha_2 P_s |\tilde{h}_{sr}|^2}{\varsigma \alpha_1 P_s |\tilde{h}_{sr}|^2 + \sigma_\epsilon^2 P_s + \sigma_\epsilon^2 P_s k_{sr}^2 + |\tilde{h}_{sr}|^2 P_s k_{sr}^2 + \frac{N_0}{2}}, \tag{10}$$

where ς denotes the residual SIC factor.

On the other hand, in the cooperative schemes, the R implements an SIC process to obtain both users' symbols. Then, R implements a new SC signal and forwards it by the power of the R to the users in the second phase. Again, R distributes the values of the power coefficient according to channel gain as in S. The received signal at u1 and u2 in the second phase is given as

$$y_{ri} = (\tilde{h}_{ri} + e)(\sqrt{P_r} s_{sc} + \eta_{ri}) + n, \tag{11}$$

where P_r is the R transmit power and $\eta_{ri} \sim \mathcal{CN}(0,\ k_{ri}^2 P_r)$.

In CNOMA, the users receive only the second phase signal; hence, they decode their messages according to y_{ri} (11) by using MLD for the m_1 and SIC process for the m_2 symbols. The SINRs for detecting m_1 (at u1 and at u2 [to enable SIC]) and m_2 (at u2) are defined, respectively, as

$$\gamma_1^{r1} = \frac{\alpha_1 P_r |\tilde{h}_{r1}|^2}{\alpha_2 P_r |\tilde{h}_{r1}|^2 + \sigma_\epsilon^2 P_r + \sigma_\epsilon^2 P_r k_{r1}^2 + |\tilde{h}_{r1}|^2 P_r k_{r1}^2 + \frac{N_0}{2}}, \tag{12}$$

$$\gamma_1^{r2} = \frac{\alpha_1 P_r |\tilde{h}_{r2}|^2}{\alpha_2 P_r |\tilde{h}_{r2}|^2 + \sigma_\epsilon^2 P_r + \sigma_\epsilon^2 P_r k_{r2}^2 + |\tilde{h}_{r2}|^2 P_r k_{r2}^2 + \frac{N_0}{2}}, \tag{13}$$

$$\gamma_2^{r2} = \frac{\alpha_2 P_r |\tilde{h}_{r2}|^2}{\varsigma \alpha_1 P_r |\tilde{h}_{r2}|^2 + \sigma_\epsilon^2 P_r + \sigma_\epsilon^2 P_r k_{r2}^2 + |\tilde{h}_{r2}|^2 P_r k_{r2}^2 + \frac{N_0}{2}}. \tag{14}$$

However, in CNOMA-WDL, the users receive signals in both phases. Thus, the users first implement an MRC by using y_{si} (1) and y_{ri} (11), then, they implement a proper detection scheme (e.g., MLD or SIC). The SINRs of m_1 and m_2 at the u1 and u2 using the MRC is given as

$$\gamma_1^{\text{CNOMA-WDL}} = \gamma_1{}^{s1} + \gamma_1{}^{r1}, \tag{15}$$
$$\gamma_{2\to1}^{\text{CNOMA-WDL}} = \gamma_1{}^{s2} + \gamma_1{}^{r2}, \tag{16}$$
$$\gamma_2^{\text{CNOMA-WDL}} = \gamma_2{}^{s2} + \gamma_2{}^{r2}. \tag{17}$$

III. PERFORMANCE ANALYSIS

A. BER ANALYSIS

In this subsection, we derive the BER expressions of NOMA, CNOMA and CNOMA-WDL for both users over Rayleigh fading channels. The binary phase-shift keying (BSPK) modulation is used to modulate the message of u1 and u2 at S and R. The e2e BER expressions in the CNOMA for both users are given as [34]

$$P_{e2e,i}^{(\text{CNOMA})} = P_{m_i,sr}\left(1 - P_{m_i,ri}\right) + \left(1 - P_{m_i,sr}\right) P_{m_i,ri}, \tag{18}$$

where $P_{m_i,sr}$ is the BER of the u1 and u2 symbols in R at the first phase, $P_{m_i,ri}$ is the BER of u1 and u2 in the second phase.

On the other hand, the e2e BER expressions in CNOMA-WDL for both users are given as [41] by

$$\begin{aligned} &P_{e2e,i}^{(\text{CNOMA-WDL})} \\ &\quad = \frac{1}{2} \sum_f g_f [P_{m_i,\text{prop}} \times P_{m_i,sr} + (1 - P_{m_i,sr}) P_{m_i,\text{coop}}], \\ &f = z,\ v, \end{aligned} \tag{19}$$

where g_f, $f = z, v$ is a parameter for u1 and u2, respectively, which is determined according to modulation order.[1] $P_{m_1,\text{prop}}$ is the BER in the presence of error propagation from R to users achieved by the MRC and $P_{m_i,\text{coop}}$ is the BER when the symbols of users are detected correctly at the R and forwarded to the users and then combined with MRC at the users.

1) BER OF NOMA FOR POINT-TO-POINT (P2P) COMMUNICATION

In P2P communication, each node (i.e., R, u1 and u2) performs an MLD to detect m_1 symbol. Thus, the BER for m_1 symbols in the presence of the effects of HWI and ipCSI is given as

$$P_{m_1,j} = \frac{1}{2}\sum_{z=1}^{2} \mathrm{Q}\left(\sqrt{2\delta_{m1,j,z}}\right),\ j = sr,\ s1,\ r1, \tag{20}$$

where $\delta_{m1,j,z}$ defined as

$$\delta_{m_1,sr,z} = \frac{P_s\psi_z|\tilde{h}_{sr}|^2}{N_0 + 2P_sk_{sr}^2|\tilde{h}_{sr}|^2 + 2(k_{sr}^2+\psi_z)P_s\sigma_\epsilon^2},$$
$$\delta_{m_1,s1,z} = \frac{P_s\psi_z|\tilde{h}_{s1}|^2}{N_0 + 2P_sk_{s1}^2|\tilde{h}_{s1}|^2 + 2(k_{s1}^2+\psi_z)P_s\sigma_\epsilon^2}, \delta_{m_1,r1,z}$$
$$= \frac{P_r\psi_z|\tilde{h}_{r1}|^2}{N_0 + 2P_rk_{r1}^2|\tilde{h}_{r1}|^2 + 2(k_{r1}^2+\psi_z)P_r\sigma_\epsilon^2},$$

in which $\psi_z = [(\sqrt{\alpha_1}+\sqrt{\alpha_2})^2, (\sqrt{\alpha_1}-\sqrt{\alpha_2})^2]$ is given according to modulation order.

Proof: Please see Appendix A. ∎

The derivation of the average BER (ABER) is defined as follows

$$P_{m_1,j} = \frac{1}{4}\sum_{z}^{2}\left(1 - \sqrt{\frac{\bar{\delta}_{m1,j,z}}{1+\bar{\delta}_{m1,j,z}}}\right), \tag{21}$$

where $\bar{\delta}_{m_1,j,z} = \mathrm{E}[\delta_{m_1,j,z}]$, E[.] is an expectation operator. Thus, $\bar{\delta}_{m_1,j,z} = \frac{P_s\psi_z\sigma_{\tilde{h}_{ij}}^2}{N_0+2P_sk_j^2\sigma_{\tilde{h}_{ij}}^2+2(k_j^2+\psi_z)P_s\sigma_\epsilon^2}$ is given.

As explained above, (21) gives the BER for a P2P NOMA scheme. Thus, it refers to BER of m_1 symbols in downlink NOMA (i.e., $P_{m_1,s1} \triangleq P_{e2e,1}^{(\text{NOMA})}$), the BER of m_1 symbols in the first phase of CNOMA and CNOMA-WDL (i.e., $P_{m_1,sr}$), and the BER of m_1 symbols in the second phase of CNOMA (i.e., $P_{m_1,r1}$). To detect m_2 symbols, each node implements a SIC process. The BER of m_2 symbols at each node is obtained as the sum of the correct and erroneous detection of the m_1 symbols during the SIC process. Therefore, by also considering the ipSIC, the BER of m_2 at R and u2 is given by

$$P_{m_2,l} = \frac{1}{2}\sum_{v=1}^{6} g_v\mathrm{Q}\left(\sqrt{2\delta_{m_2,l,v}}\right),\ \text{where } l = sr,\ s2,\ r2, \tag{22}$$

[1]These parameters change according to used modulation order and user (e.g., whether a SIC will be applied or not), and the details of deductions are given in related appendices.

where $\mathbf{g}_v = [1, 1, -1, 1, 1, -1]$, and

$$\delta_{m_2,sr,v} = \frac{P_s\zeta_v|\tilde{h}_{sr}|^2}{N_0 + 2P_sk_{sr}^2|\tilde{h}_{sr}|^2 + 2(k_{sr}^2+\xi_v)P_s\sigma_\epsilon^2},$$
$$\delta_{m_2,s2,v} = \frac{P_s\zeta_v|\tilde{h}_{s2}|^2}{N_0 + 2P_sk_{s2}^2|\tilde{h}_{s2}|^2 + 2(k_{s2}^2+\xi_v)P_s\sigma_\epsilon^2},$$
$$\delta_{m_2,r2,v} = \frac{P_r\zeta_v|\tilde{h}_{r2}|^2}{N_0 + 2P_rk_{r2}^2|\tilde{h}_{r2}|^2 + 2(k_{r2}^2+\xi_v)P_r\sigma_\epsilon^2},$$
$$\boldsymbol{\zeta}_v = [\alpha_2, \alpha_2, (\sqrt{\alpha_1}+\sqrt{\alpha_2})^2, (2\sqrt{\alpha_1}+\sqrt{\alpha_2})^2,$$
$$\times(\sqrt{\alpha_1}-\sqrt{\alpha_2})^2, (2\sqrt{\alpha_1}-\sqrt{\alpha_2})^2],$$

and $\boldsymbol{\xi}_v = [(\sqrt{\alpha_1}+\sqrt{\alpha_2})^2, (\sqrt{\alpha_1}-\sqrt{\alpha_2})^2, (\sqrt{\alpha_1}+\sqrt{\alpha_2})^2, (\sqrt{\alpha_1}+\sqrt{\alpha_2})^2, (\sqrt{\alpha_1}-\sqrt{\alpha_2})^2, (\sqrt{\alpha_1}-\sqrt{\alpha_2})^2]$.

In the definition of ζ_v, both correct and erroneous SIC conditions are considered. In the case of erroneous SIC, the erroneous detected m_1 symbols are subtracted from the received signal, thus the decision rule for detection is shifted. Hence, a few terms in ζ_v have the coefficient of 2 which occurs due to the ipSIC (The details are given in Appendix B). By using the moment generating function (MGF) and alternate form of Q(.) function, the ABER of m_2 is expressed as

$$P_{m_2,l} = \frac{1}{4}\sum_{v=1}^{6} g_v\left(1 - \sqrt{\frac{\bar{\delta}_{m_2,l,v}}{1+\bar{\delta}_{m_2,l,v}}}\right), \tag{23}$$

where $\bar{\delta}_{m_2,j,v} = \mathrm{E}[\delta_{m_2,j,v}]$,
$\bar{\delta}_{m_2,j,v} = \frac{P_s\zeta_v\sigma_{\tilde{h}_{ij}}^2}{N_0+2P_sk_j^2\sigma_{\tilde{h}_{ij}}^2+2(k_j^2+\xi_v)P_s\sigma_\epsilon^2}$.

Proof: Please see Appendix B. ∎

As discussed for u1, the BER in (23) gives the error probability of NOMA for P2P communication. Therefore, it refers to BER of m_2 symbols in downlink NOMA i.e., ($P_{m_2,s2} \triangleq P_{e2e,2}^{(\text{NOMA})}$), the BER of m_2 symbols in the first phase of CNOMA and CNOMA-WDL (i.e., $P_{m_2,sr}$), and the BER of m_2 symbols in the second phase of CNOMA (i.e., $P_{m_2,r2}$).

2) BER OF COOPERATIVE DIVERSITY WITH MRC

1) At u1: Based on the detected signals in the first phase, R implements a new SC signal again and sends it to u1 and u2 by its power. Thus, u1 and u2 receive two signals from different sources, one from S and one from R. To improve the users' messages, the users perform an MRC to combine the received signals from the two different phases. The BER of the u1 with diversity combining of the two branches using MRC is given by [41] and [42, pp. 320-321]

$$P_{m_1,\text{coop}} = \mathrm{Q}\left(\sqrt{2(\delta_{m_1,s1,z}+\delta_{m_1,r1,z})}\right). \tag{24}$$

The ABER for cooperative MRC of two branches at u1 when the mean of SNRs of branches are different (i.e., $\bar{\delta}_{m1,s1,z} \neq \bar{\delta}_{m1,r1,z}$) is given as in (25), shown at the bottom of the next page.

2) At u2: The u2 detects m_1 firstly after combining the received signals with MRC. Thereafter, using the SIC detects

its symbols m_2. The BER for MRC after the SIC to detect u2 symbols is expressed by [41] and [42, pp. 320-321]

$$P_{m_2,\text{coop}} = \text{Q}\left(\sqrt{2(\delta_{m_2,s2,v} + \delta_{m_2,r2,v})}\right). \tag{26}$$

The ABER for cooperative MRC of two branches at u2 when the mean of the SNRs of branches are different (i.e., $\bar{\delta}_{m_2,s2,v} \neq \bar{\delta}_{m_2,r2,v}$) is expressed by [41] and [43, pp. 846-847] as in (27), shown at the bottom of the page.

3) BER OF COOPERATIVE MRC WITH ERROR PROPAGATION

Unless a genie-aided relaying is implemented, the R node forwards the detected signals to the users. By considering the ipSIC, R can also detect symbols erroneously. Therefore, the erroneous symbols in R are also forwarded to the users. This phenomenon is called error propagation. These erroneous symbols are also combined with the signals received from the direct path. After the implantation of the MRC, we should describe the total received signal in order to acquire the BER in case of error propagation from u1 and u2. Without loss of the generality, we assume that the S sent a symbol $(+1)$ and a symbol $(+1)$ for u1 and u2, respectively. During the SIC process in R, the symbol of u1 is detected erroneously as (-1). Thus, after the SIC process, the symbol of the u2 is detected erroneously also as (-1).

a: AT u1

Consequently, the sum of the received signals at the u1 by MRC is given as

$$\begin{aligned}\varphi_{m_1,\text{coop}} &= \tilde{h}_{s1}^{*} y_1 + \tilde{h}_{r1}^{*} y_{r1} \\ &= (\varphi_{m_1,s1,z} - \varphi_{m_1,r1,z}) + \tilde{n}_a,\end{aligned} \tag{28}$$

where $\varphi_{m_1,s1,z}$=$P_s\psi_z|\tilde{h}_{s1}|^2$ and we define $\varphi_{m_1,r1,z} = P_r\psi_z|\tilde{g}_{r1}|^2$. However, $\tilde{n}_a$ is the effective noise with $\mathbf{E}[\tilde{n}_a] \sim \mathcal{CN}(0, \frac{N_0}{2}[\sigma^2_{\tilde{h}_{s1}} + \sigma^2_{\tilde{h}_{r1}}] + k^2_{s1}P_s\sigma_{\tilde{h}^2_{s1}}\sigma^2_\epsilon + k^2_{s1}P_s\sigma^2_{\tilde{h}_{s1}} + k^2_{r1}P_r\sigma^2_{\tilde{h}_{r1}}\sigma_\epsilon{}^2 + k^2_{r1}P_r\sigma^2_{\tilde{h}_{r1}} + \tau_{m_1,s1,z}\sigma^2_{\tilde{h}_{s1}}\sigma^2_\epsilon + \tau_{m_1,r1,z}\sigma^2_{\tilde{h}_{r1}}\sigma^2_\epsilon)$, where $\tau_{m_1,s1,z} = P_s\psi_z$, and $\tau_{m_1,r1,z} = P_r\psi_z$.

Through the MLD decision rule at the u1, $m_1 = +1$ is declared if $\varphi_{m1,\text{coop}} \geq 0$. Thus, the BER of the error propagation for the u1 symbols is defined as

$$\begin{aligned}P_{m_1,\text{prop}} &= P(\varphi_{m_1,s1,z} - \varphi_{m_1,r1,z} < \tilde{n}_a) \\ &= \text{Q}\left(\frac{\varphi_{m_1,s1,z} - \varphi_{m_1,r1,z}}{\sqrt{\omega_a}}\right),\end{aligned} \tag{29}$$

where $\omega_a = \frac{N_0}{2}[\sigma^2_{\tilde{h}_{s1}} + \sigma^2_{\tilde{h}_{r1}}] + k^2_{s1}P_s\sigma^2_{\tilde{h}_{s1}}\sigma^2_\epsilon + k^2_{s1}P_s\sigma^2_{\tilde{h}_{s1}} + k^2_{r1}P_r\sigma^2_{\tilde{h}_{r1}}\sigma_\epsilon{}^2 + k^2_{r1}P_r\sigma^2_{\tilde{h}_{r1}} + \tau_{m_1,s1,z}\sigma^2_{\tilde{h}_{s1}}\sigma^2_\epsilon + \tau_{m_1,r1,z}\sigma^2_{\tilde{h}_{r1}}\sigma^2_\epsilon$.

From (29), we can see that if R forwards an incorrect symbol, this dominates the erroneous detection rather than the additive noise. Therefore, according to [41], we can approximate the BER as $\varphi_{m_1,s1,z} - \varphi_{m_1,r1,z} < 0$ since it is likely to be an incorrect decision when the propagation error (i.e., from relay to user) dominates the received signal from DL regardless of the additive noise. The BER under error propagation is given as

$$P_{m_1,\text{prop}} = P(\varphi_{m_1,s1,z} - \varphi_{m_1,r1,z} < 0). \tag{30}$$

By averaging (30) over $\varphi_{m_1,s1,z}$and $\varphi_{m_1,r1,z}$, the average error probability under error propagation is obtained as

$$P_{m_1,\text{prop}} = \frac{\bar{\varphi}_{m_1,r1,z}}{\bar{\varphi}_{m_1,r1,z} + \bar{\varphi}_{m_1,s1,z}}, \tag{31}$$

where $\bar{\varphi}_{m_1,s1,z} = \text{E}[\varphi_{m_1,s1,z}] = P_s\psi_z\sigma^2_{\tilde{h}_{s1}}$ and $\bar{\varphi}_{m_1,r1,z} = \text{E}[\varphi_{m_1,r1,z}] = P_r\psi_z\sigma^2_{\tilde{h}_{r1}}$.

b: AT u2

Also, after combining the S and R signals at the u2, the total received signal by u2 is given as

$$\varphi_{m_2,\text{coop}} = \tilde{h}_{s2}^{*} y_2 + \tilde{h}_{r2}^{*} y_{r2}. \tag{32}$$

After the implementation of the MRC in u2, it detects the u1 symbols first, then it detects its symbols through the SIC process. Therefore, the sum of the received signal at u2 can be indicated as

$$\varphi_{m_2,\text{coop}} = (\varphi_{m_2,s2,v} - \varphi_{m_2,r2,v}) + \tilde{n}_b, \tag{33}$$

where $\varphi_{m_2,s2,v} = P_s\zeta_v|\tilde{h}_{s2}|^2$ and $\varphi_{m_2,r2,v} = P_r\zeta_v|\tilde{h}_{r2}|^2$. $\tilde{n}_b$ is the effective noise with $\mathbf{E}[\tilde{n}_b] \sim \mathcal{CN}(0, \frac{N_0}{2}[\sigma^2_{\tilde{h}_{s2}} + \sigma^2_{\tilde{h}_{r2}}] + k^2_{s2}P_s\sigma^2_{\tilde{h}_{s2}}\sigma^2_\epsilon + k^2_{s2}P_s\sigma^2_{\tilde{h}_{s2}} + k^2_{r2}P_r, \sigma^2_{\tilde{h}_{r2}}\sigma_\epsilon{}^2 + k^2_{r2}P_r\sigma^2_{\tilde{h}_{r2}} + \tau_{m_2,s2,v}\sigma^2_{\tilde{h}_{s2}}\sigma^2_\epsilon + \tau_{m_2,r2,v}\sigma^2_{\tilde{h}_{r2}}\sigma^2_\epsilon)$, where $\tau_{m_2,s2,v} = P_s\zeta_v$, and $\tau_{m_2,r2,v} = P_r\zeta_v$.

Through the MLD decision rule and the SIC process at the u2 are declared as $m_1 = +1$ and $m_2 = +1$. Thus, the BER of the error propagation for the u2 symbols is defined as

$$\begin{aligned}P_{m_2,\text{prop}} &= P(\varphi_{m_2,s2,v} - \varphi_{m_2,r2,z} < \tilde{n}_b) \\ &= \text{Q}\left(\frac{\varphi_{m_2,s2,v} - \varphi_{m_2,r2,v}}{\sqrt{\omega_b}}\right),\end{aligned} \tag{34}$$

$$P_{m_1,\text{coop}} = \frac{1}{2}\left(1 - \frac{1}{\bar{\delta}_{m_1,s1,z} - \bar{\delta}_{m_1,r1,z}}\left(\bar{\delta}_{m_1,s1,z}\sqrt{\frac{\bar{\delta}_{m_1,s1,z}}{1+\bar{\delta}_{m_1,s1,z}}} - \bar{\delta}_{m_1,r1,z}\sqrt{\frac{\bar{\delta}_{m_1,r1,z}}{1+\bar{\delta}_{m_1,r1,z}}}\right)\right). \tag{25}$$

$$P_{m_2,\text{coop}}\{s_{sc} \in v\} = \frac{1}{2}\left(1 - \frac{1}{\bar{\delta}_{m_2,s2,v} - \bar{\delta}_{m_2,r2,v}}\left(\bar{\delta}_{m_2,s2,v}\sqrt{\frac{\bar{\delta}_{m_2,s2,v}}{1+\bar{\delta}_{m_2,s2,v}}} - \bar{\delta}_{m_2,r2,v}\sqrt{\frac{\bar{\delta}_{m_2,r2,v}}{1+\bar{\delta}_{m_2,r2,v}}}\right)\right). \tag{27}$$

where $\omega_b = \frac{N_0}{2}[\sigma^2_{\tilde{h}_{s2}} + \sigma_{\tilde{h}_{r2}^2} + k^2_{s2}P_s\sigma^2_{\tilde{h}_{s2}}\sigma^2_\epsilon + k^2_{s2}P_s\sigma^2_{\tilde{h}_{s2}} + k^2_{r2}P_r\sigma^2_{\tilde{h}_{r2}}\sigma_\epsilon{}^2 + k^2_{r2}P_r\sigma^2_{\tilde{h}_{r2}} + \tau_{m_2,s2,v}\sigma^2_{\tilde{h}_{s2}}\sigma^2_\epsilon + \tau_{m_2,r2,v}\sigma^2_{\tilde{h}_{r2}}\sigma^2_\epsilon$.

As discussed above, similarly, we can see from (34) that the propagation error has a dominant effect on the decision of m_2 symbols. In other words, if R forwards an incorrect symbol, the decision during MLD and SIC is likely to be erroneous regardless of the additive noise. Consequently, we can approximate the BER for the SIC to detect m_2 as $\varphi_{m_2,s2,v} - \varphi_{m_2,r2,v} < 0$ [41], and the BER under error propagation is obtained as

$$P_{m_2,\text{prop}} = P(\varphi_{m_2,s2,v} - \varphi_{m_2,r2,v} < 0). \tag{35}$$

By averaging (35) over $\varphi_{m_2,s2,v}$ and $\varphi_{m_2,r2,v}$, the average error probability under error propagation is obtained as

$$P_{m_2,\text{prop}} = \frac{\bar{\varphi}_{m_2,r2,v}}{\bar{\varphi}_{m_2,r2,v} + \bar{\varphi}_{m_2,s2,v}}, \tag{36}$$

where $\bar{\varphi}_{m_2,s2,v} = \text{E}[\varphi_{m_2,s2,v}] = P_s\zeta_v\sigma^2_{\tilde{h}_{s2}}$ and $\bar{\varphi}_{m_2,s2,v} = \text{E}[\varphi_{m_2,r2,v}] = P_r\zeta_v\sigma^2_{\tilde{h}_{r2}}$.

Finally, to find the e2e BER in CNOMA, we obtain $P_{m_1,sr}$, $P_{m_1,r1}$ by using (21) and $P_{m_2,sr}$, $P_{m_1,r2}$ by using (23) and then substituting them into (18) for u1 and u2, respectively.

On the other hand, to obtain the e2e BER in CNOMA-WDL, we determine $P_{m_1,sr}$, $P_{m_1,\text{coop}}$, and $P_{m_1,\text{prop}}$ by using (21), (25), and (31), and substitute them into (19) for u1. Similarly, we determine $P_{m_2,sr}$, $P_{m_2,\text{coop}}$, and $P_{m_2,\text{prop}}$ by using (23), (27), and (36), and substitute them into (19) for u2.

4) BER OF SYSTEM

In our considered scenarios, the BER of system is the error probability when the u1, u2 or both detect their own symbols erroneously. Thus, the BER of system of NOMA, CNOMA and CNOMA-WDL can be expressed respectively as [44] and [45]

$$P^{NOMA}_{sys} = 1 - \left(1 - P_{m_1,s1}\right)\left(1 - P_{m_2,s2}\right), \tag{37}$$

$$P^{CNOMA}_{sys} = 1 - \left(1 - P^{(\text{CNOMA})}_{e2e,1}\right)\left(1 - P^{(\text{CNOMA})}_{e2e,2}\right), \tag{38}$$

$$P^{CNOMA-WDL}_{sys} = 1 - \left(1 - P^{(\text{CNOMA-WDL})}_{e2e,1}\right) \times \left(1 - P^{(\text{CNOMA-WDL})}_{e2e,2}\right), \tag{39}$$

where $P_{m_1,s1}$ and $P_{m_2,s2}$ are the BER of NOMA for u1 and u2 respectively, $P^{(\text{CNOMA})}_{e2e,1}$ and $P^{(\text{CNOMA})}_{e2e,2}$ are the BER of CNOMA for u1 and u2 respectively, $P^{(\text{CNOMA-WDL})}_{e2e,1}$ and $P^{(\text{CNOMA-WDL})}_{e2e,2}$ are the BER of CNOMA-WDL for u1 and u2 respectively.

B. OUTAGE PROBABILITY ANALYSIS

In this subsection, we derive the OP expressions for different NOMA schemes: NOMA, CNOMA and CNOMA-WDL over Rayleigh fading channel. In general, the OP of CNOMA without a DL can be given as

$$P^{(\text{CNOMA})}_{e2e,i}(out) = 1 - \left(1 - P_{m_i,sr}(out)\right)\left(1 - P_{m_i,ri}(out)\right),\ i = 1,\ 2, \tag{40}$$

where, the $P_{m_i,sr}(out)$ is the OP of m_1 and m_2 symbols at the R in the first phase, $P_{m_i,ri}(out)$ is the OP m_1 and m_2 symbols at users in the second phase.

1) OP OF NOMA FOR P2P

The outage of m_1 at u1 and R occurs if the received SINR of m_1 is less than the threshold. Hence, by using probability density function (PDF) and cumulative distribution function (CDF) as [46, eq. (7) and (8)], the OP[2] of the m_1 at u1 and R under HWI, ipCSI and ipSIC is expressed as [49]

$$P_{m_1,j}(out) = P\left(\gamma^j_1 \le \gamma_{th,1}\right) = 1 - \exp\left(-\gamma_{th,1}\tau^j_1\right),\ j = sr, s1, r1, \tag{41}$$

where $\tau^{sr}_1 = \frac{\left(\frac{N_0}{2} + \sigma^2_\epsilon P_s + \sigma^2_\epsilon P_s k_{sr}{}^2\right)}{\Phi_{sr}\left(\alpha_1 P_s - \gamma_{th,1}P_s\alpha_2 - \gamma_{th,1}P_s k_{sr}{}^2\right)}$,
$\tau^{s1}_1 = \frac{\left(\frac{N_0}{2} + \sigma^2_\epsilon P_s + \sigma^2_\epsilon P_s k_{s1}{}^2\right)}{\Phi_{s1}\left(\alpha_1 P_s - \gamma_{th,1}P_s\alpha_2 - \gamma_{th,1}P_s k_{s1}{}^2\right)}$,
$\tau^{r1}_1 = \frac{\left(\frac{N_0}{2} + \sigma^2_\epsilon P_r + \sigma^2_\epsilon P_r k_{r1}{}^2\right)}{\Phi_{r1}\left(\alpha_1 P_r - \gamma_{th,1}P_r\alpha_2 - \gamma_{th,1}P_r k_{r1}{}^2\right)}$, and
$\Phi_j = \text{E}[|\tilde{h}_j|^2]$ are defined. $\gamma_{th,1} = 2^{\Xi R_1} - 1$ is the threshold of m_1, and Ξ is the time slot equal to 1 for NOMA and 2 for CNOMA.

Proof: Please see Appendix C. ■

Likewise, the outage of m_2 occurs if one of the two events occurs: If u2 and R fails to detect m_1 and if m_1 is successfully detected and fails to detect m_2. By using PDF and CDF [46, eq. (7) and (8)], the OP of m_2 at u2 and R with HWI, ipCSI and ipSIC is determined as

$$P_{m_2,l}(out) = P\left(\gamma^l_1 \le \gamma_{th,1}\right) + P\left(\gamma^l_1 > \gamma_{th,1}\right)P\left(\gamma^l_2 \le \gamma_{th,2}\right) = 1 - \exp\left(-\tau^l_1\gamma_{th,1}\right)\exp\left(-\tau^l_2\gamma_{th,2}\right),\ l = sr, s2, r2, \tag{42}$$

where $\tau^{sr}_2 = \frac{\left(\frac{N_0}{2} + \sigma^2_\epsilon P_s + \sigma^2_\epsilon P_s k_{sr}{}^2\right)}{\Phi_{sr}\left(\alpha_2 P_s - \varsigma\gamma_{th,2}P_s\alpha_1 - \gamma_{th,2}P_s k_{sr}{}^2\right)}$,
$\tau^{s2}_1 = \frac{\left(\frac{N_0}{2} + \sigma^2_\epsilon P_s + \sigma^2_\epsilon P_s k_{s2}{}^2\right)}{\Phi_{s2}\left(\alpha_1 P_s - \gamma_{th,1}P_s\alpha_2 - \gamma_{th,1}P_s k_{s2}{}^2\right)}$,
$\tau^{s2}_2 = \frac{\left(\frac{N_0}{2} + \sigma^2_\epsilon P_s + \sigma^2_\epsilon P_s k_{s2}{}^2\right)}{\Phi_{s2}\left(P_s\alpha_2 - \gamma_{th,2}\varsigma\alpha_1 P_s - \gamma_{th,2}P_s k_{s2}{}^2\right)}$,
$\tau^{r2}_1 = \frac{\left(\frac{N_0}{2} + \sigma^2_\epsilon P_r + \sigma^2_\epsilon P_r k_{r2}{}^2\right)}{\Phi_{r2}\left(\alpha_1 P_r - \gamma_{th,1}P_r\alpha_2 - \gamma_{th,1}P_r k_{r2}{}^2\right)}$,
$\tau^{r2}_2 = \frac{\left(\frac{N_0}{2} + \sigma^2_\epsilon P_r + \sigma^2_\epsilon P_r k_{r2}{}^2\right)}{\Phi_{r2}\left(P_r\alpha_2 - \gamma_{th,2}\varsigma\alpha_1 P_r - \gamma_{th,2}P_r k_{r2}{}^2\right)}$, and $\Phi_l = \text{E}[|\tilde{h}_l|^2]$ are defined. $\gamma_{th,2}$ is the threshold of m_2, $\gamma_{th,2} = 2^{\Xi R_2} - 1$.

[2]The statistical CSI at each link is assumed to be available at each node, whereas the nodes have access to the ipCSI of their respective channel links. Thus, without loss of generality, the effective channel gains of users are sorted as $E[|\tilde{h}_{s1}|^2] < E[|\tilde{h}_{s2}|^2]$. Therefore, the PDF and CDF of statistically channel gains of one and any two independent random variables are defined in [34], [35], [46], [47], and [48].

2) OUTAGE PROBABILITY OF THE CNOMA-WDL

The u1 implement an MRC to combine the two received signal from S and R. Hence, the e2e OP expression of the CNOMA-WDL is given by [47]

$$P_1^{\text{CNOMA-WDL}}(out) = (1 - P(\gamma_1{}^{sr} < \gamma_{th,1}))P(\gamma_1^{\text{CNOMA}} < \gamma_{th,1}) + P(\gamma_1{}^{sr} < \gamma_{th,1})P(\gamma_1^{s1} < \gamma_{th,1}). \quad (43)$$

The terms $P(\gamma_1{}^{sr} < \gamma_{th,1}) \triangleq P_{m_1,sr}(out)$ and $P(\gamma_1^{s1} < \gamma_{th,1}) \triangleq P_{m_1,s1}(out)$ are given in (41), where Ξ=2. The term $P(\gamma_1^{\text{CNOMA}} < \gamma_{th,1})$ consists of two independent exponential random variables γ_1^{r1} and γ_1^{s1}. Thus, by using the CDF of two independent exponential random variables (RVs) γ_1^{r1} and γ_1^{s1} as in [47, eq. (6)], the OP of m_1 when $\gamma_1^{r1} \neq \gamma_1^{s1}$ can be expressed as (44), shown at the bottom of the page.

By substituting $P(\gamma_1{}^{sr} < \gamma_{th,1})$, $P(\gamma_1^{s1} < \gamma_{th,1})$ and $P(\gamma_1^{\text{CNOMA}} < \gamma_{th,1})$, from (41) and (44) into (43), we get the OP of the u1 for the CNOMA-WDL as in (45), shown at the bottom of the page.

The OP at the output MRC for u2 occurs if one of two cases events: If m_1 is failing detected at output MRC and if m_1 is correctly detected and m_2 is failing detected at output MRC. Thus, the OP of the m_2 at the u2 at output MRC is given by

$$P_2(out) = P_{2\to1}^{\text{CNOMA-WDL}}(out) + \left[1 - P_{2\to1}^{\text{CNOMA-WDL}}(out)\right] P_2^{\text{CNOMA-WDL}}(out), \quad (46)$$

where $P_{2\to1}^{\text{CNOMA-WDL}}(out)$ is the OP at output MRC to detect m_1 at u2 and $P_2^{\text{CNOMA-WDL}}(out)$ is the OP at output MRC to detect m_1 at u2. Thus, OP to detect m_1 at u2 at output MRC is given by

$$P_{2\to1}^{\text{CNOMA-WDL}}(out) = (1 - P\left(\gamma_1{}^{sr} < \gamma_{th,1}\right))P\left(\gamma_{2\to1}^{\text{CNOMA}} < \gamma_{th,1}\right) + P\left(\gamma_1{}^{sr} < \gamma_{th,1}\right) P\left(\gamma_1^{s2} < \gamma_{th,1}\right). \quad (47)$$

The terms $P(\gamma_1{}^{sr} < \gamma_{th,1}) \triangleq P_{m_1,sr}(out)$ is given in (41), where Ξ=2. By using the CDF of two independent exponential RVs γ_1^{r2} and γ_1^{s2}, when $\gamma_1^{r2} \neq \gamma_1^{s2}$ as in [47, eq. (6)]. The other terms are expressed by using the CDF of one and two independent RVs as in [46, eq. (8)], [47, eq. (6)] by

$$P\left(\gamma_1^{s2} < \gamma_{th,1}\right) = 1 - \exp\left(-\tau_1^{s2}\gamma_{th,1}\right), \quad (48)$$

$$P(\gamma_{2\to1}^{\text{CNOMA}} < \gamma_{th,1}) = 1 - \left[\frac{\tau_1^{s2}}{\tau_1^{s2} - \tau_1^{r2}} \exp\left(-\tau_1^{s2}\gamma_{th,1}\right) + \frac{\tau_1^{r2}}{\tau_1^{r2} - \tau_1^{s2}} \exp\left(-\tau_1^{r2}\gamma_{th,1}\right)\right], \quad \text{where} \quad \tau_1^{s2} \neq \tau_1^{r2}. \quad (49)$$

By substituting (41), (48) and (49) into (47), we get the OP of the m_1 at output MRC at u2 as in (50), shown at the bottom of the next page.

The OP of m_2 at output MRC at u2 is given as

$$P_2^{\text{CNOMA-WDL}}(out) = (1 - P\left(\gamma_2{}^{sr} < \gamma_{th,2}\right))P\left(\gamma_2^{\text{CNOMA}} < \gamma_{th,2}\right) + P\left(\gamma_2{}^{sr} < \gamma_{th,2}\right) P\left(\gamma_2^{s2} < \gamma_{th,2}\right). \quad (51)$$

The terms of (51) are computed using the CDF of one and two independent RVs [46, eq. (8)], [47, eq. (6)] as

$$P(\gamma_2{}^{sr} < \gamma_{th,2}) = 1 - \exp\left(-\tau_2^{sr}\gamma_{th,2}\right), \quad (52)$$

$$P(\gamma_2^{s2} < \gamma_{th,2}) = 1 - \exp\left(-\tau_2^{s2}\gamma_{th,2}\right), \quad (53)$$

$$P(\gamma_2^{\text{CNOMA}} < \gamma_{th,2}) = 1 - \left[\frac{\tau_2^{s2}}{\tau_2^{s2} - \tau_2^{r2}} \exp\left(-\tau_2^{s2}\gamma_{th,2}\right) + \frac{\tau_2^{r2}}{\tau_2^{r2} - \tau_2^{s2}} \exp\left(-\tau_2^{r2}\gamma_{th,2}\right)\right], \quad \text{where } \tau_2^{s2} \neq \tau_2^{r2}. \quad (54)$$

By substituting (52), (53), and (54) into (51), we get the OP of the m_2 at output MRC at u2 as in (55), shown at the bottom of the next page.

By substituting (50) and (55) into (46), we find the OP of the u2 for the CNOMA-WDL as in (56), shown at the bottom of the next page.

3) ASYMPTOTIC OUTAGE PROBABILITY

To obtain insight into our considered scenarios, the asymptotic OP is presented in high SNR regimes (where in high

$$P(\gamma_1^{\text{CNOMA}} < \gamma_{th,1}) = 1 - \left[\frac{\tau_1^{s1}}{\tau_{s1} - \tau_{r1}} \exp\left(-\tau_1^{s1}\gamma_{th,1}\right) + \frac{\tau_1^{r1}}{\tau_1^{r1} - \tau_1^{s1}} \exp\left(-\tau_1^{r1}\gamma_{th,1}\right)\right], \text{where } \tau_1^{s1} \neq \tau_1^{r1}. \quad (44)$$

$$P_1^{\text{CNOMA-WDL}}(out) = \exp\left(-\gamma_{th,1}\tau_1^{sr}\right)\left(1 - \left[\frac{\tau_1^{s1}}{\tau_{s1} - \tau_{r1}} \exp\left(-\tau_1^{s1}\gamma_{th,1}\right) + \frac{\tau_1^{r1}}{\tau_1^{r1} - \tau_1^{s1}} \exp\left(-\tau_1^{r1}\gamma_{th,1}\right)\right]\right) + \left(1 - \exp\left(-\gamma_{th,1}\tau_1^{sr}\right)\right)\left(1 - \exp\left(-\gamma_{th,1}\tau_1^{s1}\right)\right). \quad (45)$$

SNR, we use $\exp(-x) \approx (1-x)$ as in [50]). The asymptotic OP of the m_1 at $u1$ and R can be expressed as

$$P^{\infty}_{m_1,j}(out) \approx \gamma_{th,1}\tau_1^j, \tag{57}$$

The asymptotic OP of the m_2 at $u2$ and R can be expressed as

$$P^{\infty}_{m_2,l}(out) \approx 1 - \left(1-\tau_1^l\gamma_{th,1}\right)\left(1-\tau_2^l\gamma_{th,2}\right), \tag{58}$$

The asymptotic OP of the CNOMA without DL can be presented as

$$P^{\infty,\mathsf{CNOMA}}_{e2e,i}(out) \approx 1 - \left(1-P^{\infty}_{m_i,sr}(out)\right) \times \left(1-P^{\infty}_{m_i,ri}(out)\right),\ i=1,\ 2, \tag{59}$$

where $P^{\infty}_{m_i,sr}(out)$ and $P^{\infty}_{m_i,ri}(out)$ are the asymptotic OP of the m_1 and m_2 in the first and second phase.

The asymptotic OP of u1 for the CNOMA-WDL is presented in (60), as shown at the bottom of the next page.

The asymptotic OP of u2 for the CNOMA-WDL is presented in (61), as shown at the bottom of the next page.

It is remarked that the OP performance is affected by the practical constraints (HWI, ipCSI, and ipSIC) in the high SNR regimes, which have a negative effect on the OP. The OP is dependent on HWI, ipCSI, and ipSIC in the high SNR regimes.

4) OUTAGE PROBABILITY OF SYSTEM

In our considered scenarios, the OP of system is the probability that the u1, u2 or both fail to decode their own signals. Thus, the system OP of NOMA, CNOMA and CNOMA-WDL can be expressed respectively as [44] and [45]

$$P^{\mathsf{NOMA}}_{sys}(out) = 1 - \left(1-P_{m_1,s1}(out)\right)\left(1-P_{m_2,s2}(out)\right), \tag{62}$$

$$P^{\mathsf{CNOMA}}_{sys}(out) = 1 - \left(1-P^{\mathsf{CNOMA}}_{e2e,1}(out)\right)\left(1-P^{\mathsf{CNOMA}}_{e2e,2}(out)\right), \tag{63}$$

$$P^{\mathsf{CNOMA-WDL}}_{sys}(out) = 1 - \left(1-P^{\mathsf{CNOMA-WDL}}_{1}(out)\right)\left(1-P_2(out)\right), \tag{64}$$

where $P_{m_1,s1}(out)$ and $P_{m_2,s2}(out)$ are the OP of NOMA for u1 and u2 respectively, $P^{(\mathsf{CNOMA})}_{e2e,1}(out)$ and $P^{(\mathsf{CNOMA})}_{e2e,2}(out)$ are the OP of CNOMA for u1 and u2 respectively, $P^{\mathsf{CNOMA-WDL}}_{1}(out)$ and $P_2(out)$ are the OP of CNOMA-WDL for u1 and u2 respectively.

Likewise, the asymptotic OP of system of NOMA, CNOMA and CNOMA-WDL can be expressed respectively as

$$P^{\infty,\mathsf{NOMA}}_{sys}(out) \approx 1 - \left(1-P^{\infty}_{m_1,s1}(out)\right)\left(1-P^{\infty}_{m_2,s2}(out)\right), \tag{65}$$

$$P^{\infty,\mathsf{CNOMA}}_{sys}(out) \approx 1 - \left(1-P^{\infty,\mathsf{CNOMA}}_{e2e,1}(out)\right)\left(1-P^{\infty,\mathsf{CNOMA}}_{e2e,2}(out)\right), \tag{66}$$

$$P^{\infty,\mathsf{CNOMA-WDL}}_{sys}(out) \approx 1 - \left(1-P^{\infty,\mathsf{CNOMA-WDL}}_{1}(out)\right)\left(1-P^{\infty}_{2}(out)\right), \tag{67}$$

$$P^{\mathsf{CNOMA-WDL}}_{2\to 1}(out) = \exp\left(-\tau_1^{sr}\gamma_{th,1}\right)\left(1-\left[\frac{\tau_1^{s2}}{\tau_1^{s2}-\tau_1^{r2}}\exp\left(-\tau_1^{s2}\gamma_{th,1}\right)+\frac{\tau_1^{r2}}{\tau_1^{r2}-\tau_1^{s2}}\exp\left(-\tau_1^{r2}\gamma_{th,1}\right)\right]\right) + \left(1-\exp\left(-\tau_1^{sr}\gamma_{th,1}\right)\right)\left(1-\exp\left(-\tau_1^{s2}\gamma_{th,1}\right)\right). \tag{50}$$

$$P^{\mathsf{CNOMA-WDL}}_{2}(out) = \exp\left(-\tau_2^{sr}\gamma_{th,2}\right)\left(1-\left[\frac{\tau_2^{s2}}{\tau_2^{s2}-\tau_2^{r2}}\exp\left(-\tau_2^{s2}\gamma_{th,2}\right)+\frac{\tau_2^{r2}}{\tau_2^{r2}-\tau_2^{s2}}\exp\left(-\tau_2^{r2}\gamma_{th,2}\right)\right]\right) + \left(1-\exp\left(-\tau_2^{sr}\gamma_{th,2}\right)\right)\left(1-\exp\left(-\tau_2^{s2}\gamma_{th,2}\right)\right). \tag{55}$$

$$\begin{aligned} P_2(out) = {} & \exp\left(-\tau_1^{sr}\gamma_{th,1}\right)\left(1-\left[\frac{\tau_1^{s2}}{\tau_1^{s2}-\tau_1^{r2}}\exp\left(-\tau_1^{s2}\gamma_{th,1}\right)+\frac{\tau_1^{r2}}{\tau_1^{r2}-\tau_1^{s2}}\exp\left(-\tau_1^{r2}\gamma_{th,1}\right)\right]\right) + \left(1-\exp\left(-\tau_1^{sr}\gamma_{th,1}\right)\right) \\ & \times\left(1-\exp\left(-\tau_1^{s2}\gamma_{th,1}\right)\right) + \left(1-\exp\left(-\tau_1^{sr}\gamma_{th,1}\right)\right)\left(1-\left[\frac{\tau_1^{s2}}{\tau_1^{s2}-\tau_1^{r2}}\exp\left(-\tau_1^{s2}\gamma_{th,1}\right)+\frac{\tau_1^{r2}}{\tau_1^{r2}-\tau_1^{s2}}\exp\left(-\tau_1^{r2}\gamma_{th,1}\right)\right]\right) \\ & + \left(1-\exp\left(-\tau_1^{sr}\gamma_{th,1}\right)\right)\left(1-\exp\left(-\tau_1^{s2}\gamma_{th,1}\right)\right)\left(\exp\left(-\tau_2^{sr}\gamma_{th,2}\right)\right. \\ & \times\left.\left(1-\left[\frac{\tau_2^{s2}}{\tau_2^{s2}-\tau_2^{r2}}\exp\left(-\tau_2^{s2}\gamma_{th,2}\right)+\frac{\tau_2^{r2}}{\tau_2^{r2}-\tau_2^{s2}}\exp\left(-\tau_2^{r2}\gamma_{th,2}\right)\right]\right) + \left(1-\exp\left(-\tau_2^{sr}\gamma_{th,2}\right)\right)\left(1-\exp\left(-\tau_2^{s2}\gamma_{th,2}\right)\right)\right). \end{aligned} \tag{56}$$

where $P^{\infty}_{m_1,s1}(out)$ and $P^{\infty}_{m_2,s2}(out)$ are the asymptotic OP of NOMA for u1 and u2 respectively, $P^{\infty,\text{CNOMA}}_{e2e,1}(out)$ and $P^{\infty,\text{CNOMA}}_{e2e,2}(out)$ are the asymptotic OP of CNOMA for u1 and u2 respectively, $P^{\infty,\text{CNOMA}-\text{WDL}}_{1}(out)$ and $P^{\infty}_{2}(out)$ are the asymptotic OP of CNOMA-WDL for u1 and u2 respectively.

IV. NUMERICAL RESULTS

In this section, we validate the analytical BER and OP results with computer simulations for three schemes (i.e., NOMA, CNOMA, CNOMA-WDL). Unless otherwise stated, we set the parameters to $d_{h_{s1}} = 4$ m, $d_{h_{s2}} = 2$ m, $d_{h_{sr}} = 1$ m, $d_{h_{r1}} = 3$ m, $d_{h_{r2}} = 1$ m, [51] $P_r = P_s, \alpha_1 = 0.8, \alpha_2 = 0.2$ and ipSIC factor set at $\varsigma = 0.001$ [34]. The HWI level is equal for all nodes, i.e., $k_{s1} = k_{s2} = k_{r1} = k_{r2} = k$ as in [26].

In Fig. 2, we present the BER performance w.r.t. SNR where the ipCSI is considered as $\sigma^2_\epsilon = 0.005$ which is used in [52] and the HWI factor is set at $k = 0.175$ as in [53] representing the worst value of HWI in the open literature. First, it is observed that the numerical results match perfectly with the simulation results, which proves the correctness of our analysis. Based on the results, as expected, with the increase of HWI and ipCSI levels, all NOMA schemes get worse performance. By comparing NOMA schemes with the HWI, we obverse that NOMA is superior to CNOMA. This can be explained as follows. In the presence of HWI, due to the increased HWI in total (additional HWI at R node), the performance of each phase is drastically degraded, so that the e2e performance of CNOMA becomes worse than simple downlink NOMA schemes. On the other hand, CNOMA-WDL outperforms both schemes whether a HWI is introduced or not since a diversity path is achieved by MRC. Nevertheless, a full diversity order (i.e., 2) may not be observed. This is for two reasons. The first is due to error propagation from R to users. As explained in our analysis, unless a genie-aided relaying is not considered, the R node also forwards erroneous symbols to the users, which causes an error floor in high the SNR regime. The second reason of the error floor is the imperfections in the system due to HWI or ipCSI.

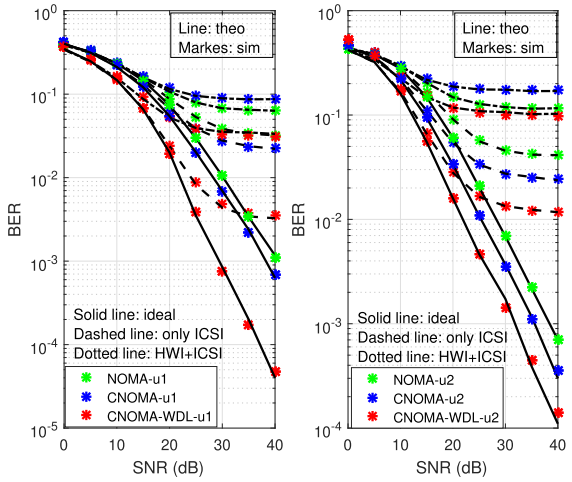

FIGURE 2. BER performances of NOMA, CNOMA and CNOMA-WDL w.r.t. SNR, when $\sigma^2_\epsilon = 0.005$.

To further evaluate the effect of HWI, in Fig. 3, we present BER performances versus the HWI level for SNR= 15, 40 dB when $\sigma^2_\epsilon = 0.005$. As expected, with increasing HWI, all schemes have a higher BER. In Fig. 3, one can easily see that the CNOMA-WDL is superior to both schemes for all HWI values. For both SNR values, the CNOMA outperforms the NOMA regardless of HWI level. In this regard, we can say that when the HWI is high, using CNOMA rather than NOMA is more beneficial.

Fig. 4. shows the effect of PA on the BER performances with different levels of HWI. It is observed that the PA affects the BER performance of one user at the expense of the other. Nevertheless, increasing α_2 too much does always not mean an increase in the performance of u2 due to the SIC process. Thus, PA should be carefully chosen not to cause unfairness for users. However, the presence of HWI degrades the BER performance of the users in all schemes despite increasing α_2.

The impact of channel estimation error on the BER performance of different NOMA schemes is evaluated in Fig. 5,

$$P^{\infty,\text{CNOMA}-\text{WDL}}_{1}(out) \approx \left(1-\gamma_{th,1}\tau_1^{sr}\right)\left(1-\left[\frac{\tau_1^{s1}}{\tau_{s1}-\tau_{r1}}\left(1-\tau_1^{s1}\gamma_{th,1}\right)+\frac{\tau_1^{r1}}{\tau_1^{r1}-\tau_1^{s1}}\left(1-\tau_1^{r1}\gamma_{th,1}\right)\right]\right)+\left(\gamma_{th,1}\tau_1^{sr}\right)\left(\gamma_{th,1}\tau_1^{s1}\right). \tag{60}$$

$$\begin{aligned} P^{\infty}_{2}(out) \approx{}& \left(1-\tau_1^{sr}\gamma_{th,1}\right)\left(1-\left[\frac{\tau_1^{s2}}{\tau_1^{s2}-\tau_1^{r2}}\left(1-\tau_1^{s2}\gamma_{th,1}\right)+\frac{\tau_1^{r2}}{\tau_1^{r2}-\tau_1^{s2}}\left(1-\tau_1^{r2}\gamma_{th,1}\right)\right]\right)+\left(\tau_1^{sr}\gamma_{th,1}\right)\\ &\times\left(\tau_1^{s2}\gamma_{th,1}\right)+\left(\left(\tau_1^{sr}\gamma_{th,1}\right)\left(1-\left[\frac{\tau_1^{s2}}{\tau_1^{s2}-\tau_1^{r2}}\left(1-\tau_1^{s2}\gamma_{th,1}\right)+\frac{\tau_1^{r2}}{\tau_1^{r2}-\tau_1^{s2}}\left(1-\tau_1^{r2}\gamma_{th,1}\right)\right]\right)+\left(\tau_1^{sr}\gamma_{th,1}\right)\left(\tau_1^{s2}\gamma_{th,1}\right)\right)\\ &\times\left(\left(1-\tau_2^{sr}\gamma_{th,2}\right)\left(1-\left[\frac{\tau_2^{s2}}{\tau_2^{s2}-\tau_2^{r2}}\left(1-\tau_2^{s2}\gamma_{th,2}\right)+\frac{\tau_2^{r2}}{\tau_2^{r2}-\tau_2^{s2}}\left(1-\tau_2^{r2}\gamma_{th,2}\right)\right]\right)+\left(\tau_2^{sr}\gamma_{th,2}\right)\left(\tau_2^{s2}\gamma_{th,2}\right)\right). \end{aligned} \tag{61}$$

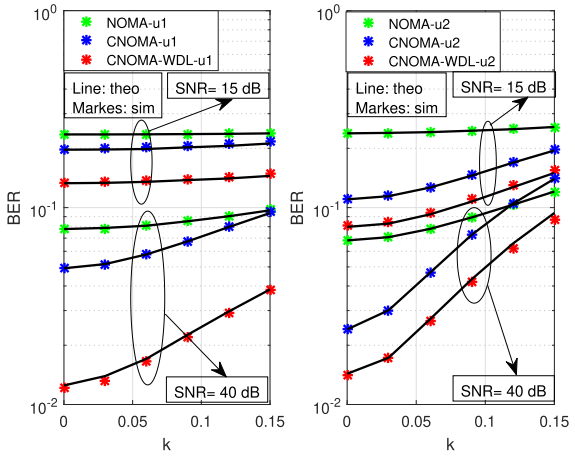

FIGURE 3. BER performances of NOMA, CNOMA and CNOMA-WDL w.r.t. HWI level, when $\sigma_\epsilon^2 = 0.005$ and SNR = 15, 40 dB.

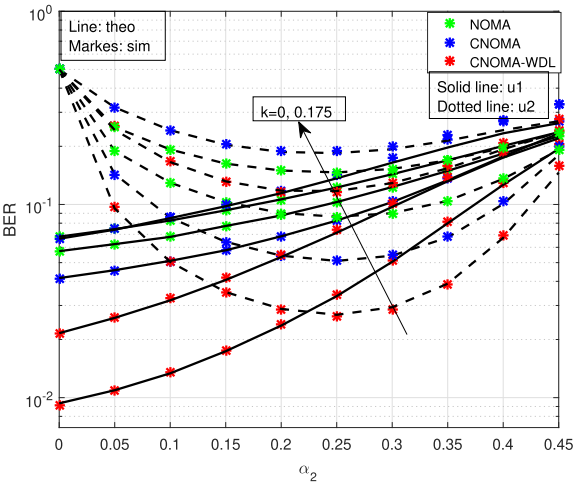

FIGURE 4. BER performances of NOMA, CNOMA and CNOMA-WDL w.r.t. PA, when $\sigma_\epsilon^2 = 0.005$ and SNR = 20 dB.

with SNR = 20 dB and different k values. As we can see that increasing ipCSI and HWI factor decrease the performance of both users, which means that the system's performance depends clearly on channel estimation error. As expected, the NOMA outperforms the CNOMA due to error propagation in the second phase.

In Fig. 6, the effect of the R position on the BER performance of the different NOMA schemes with different levels of HWI and SNR = 20 dB is presented. It is observed that the u2 achieves better performance than the u1. The change of R location affects the users' performance e.g., when the R distance is nearby the middle of both users, we achieve the best BER performance of both users. The higher distance between S and R means more errors in the first phase so the information forwarding in the second phase will be with more errors. Again, increasing k deteriorates the performance of both users, and NOMA achieves better performance than CNOMA due to error propagation in the second phase.

In order to evaluate the performance of our schemes compared to conventional OMA, we consider that OMA is employed by time division multiple access (TDMA).

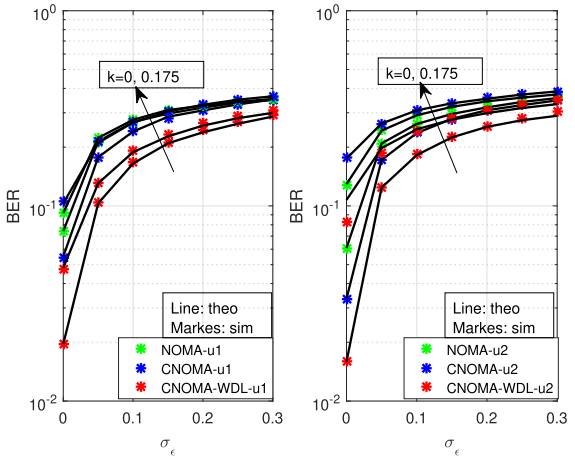

FIGURE 5. BER performances of NOMA, CNOMA and CNOMA-WDL w.r.t. σ_ϵ^2, when SNR = 20 dB.

In downlink OMA, the source transmits the users' signals within two different time slots, while in the COMA with and without direct links (COMA/COMA-WDL), there are four-time slots to transmit the users' signals. Thus, two different time slots to transmit the signals to the R and two different time slots to forward the signals from R to the users in the second phase. In the first two time slots, the source transmits the signals of u1 and u2 at different times to the R and users (in the case of COMA, the users can not receive the source signals directly; hence, they will receive their signals with the help of the R only). In the second two time slots, the R re-encodes the u1 and u2 signals and forwards them using its own power to the users in the second phase. In COMA with direct links, the u1 and u2 receive two signals from different sources (i.e., from source and R); hence, they implement the MRC to combine the received signals. In contrast, in NOMA the users' signals are combined in an SC signal at the source with different PA based on the channel gain of each user and transmitted in a single time slot. In CNOMA and CNOMA-WDL, the users' signals are transmitted in an SC signal over two-time slots that are split into phases one and two (as described in Section II). Also, based on the previous results in Fig. 6, the users achieve better performance when the relay node is nearby the middle. Thus, to satisfy a fair comparison between the two NOMA and OMA systems. We take into account the case of the best performance in both users, where the relay node is nearby the middle for both users, so, we set the distances of the BER of system at $d_{h_{s1}} = 4$m, $d_{h_{s2}} = 2$m, $d_{h_{sr}} = 1.6$m, $d_{h_{r1}} = 2.4$m, $d_{h_{r2}} = 0.4$m. A comparison between NOMA and OMA schemes under the effect of HWI and ipCSI are given in Fig,7 with $\sigma_\epsilon^2 = 0.005$ and $k = 0.175$. The BER of system is obtained as in (37), (38) and (39) for the three different schemes. It can be easily seen that the OMA outperforms NOMA schemes whether in the ideal or impaired scenarios, which refers to the fact that the NOMA schemes suffer from inter-user interference (IUI). In order to compare the effect of HWI on both NOMA and OMA schemes, in Fig. 8, we present the BER of system of the

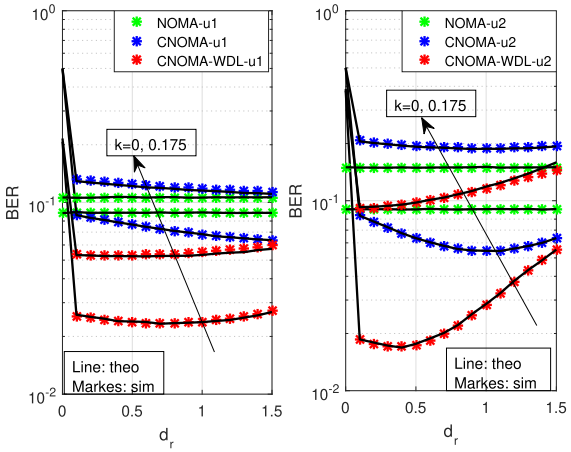

FIGURE 6. BER performances of NOMA, CNOMA and CNOMA-WDL w.r.t. d_r, when $\sigma_\epsilon^2 = 0.005$ and SNR = 20 dB.

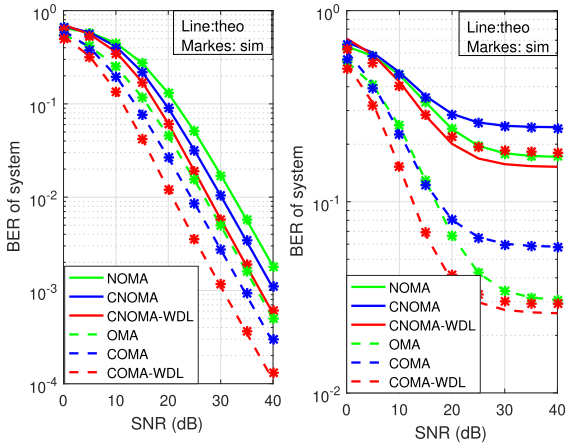

FIGURE 7. BER of system performances of NOMA and OMA w.r.t. *SNR*.

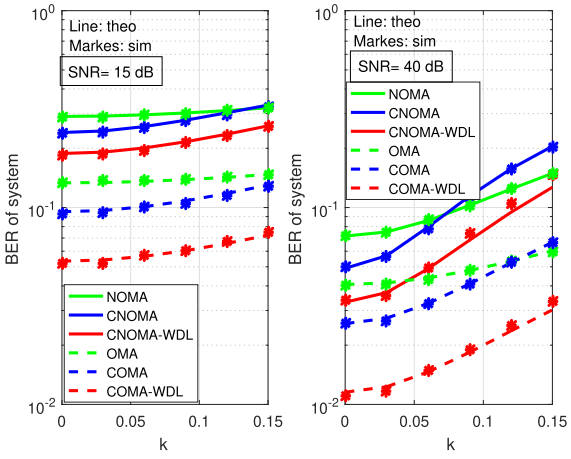

FIGURE 8. BER of system performances of NOMA and OMA w.r.t. HWI level, when $\sigma_\epsilon^2 = 0.005$ and SNR = 15, 40 dB.

NOMA and OMA versus HWI with $\sigma_\epsilon^2 = 0.005$. We can observe that the NOMA and OMA systems perform worse for both levels of SNR as the HWI factor increases. Again, the OMA schemes outperform the NOMA scheme due to the presence of IUI in the NOMA system.

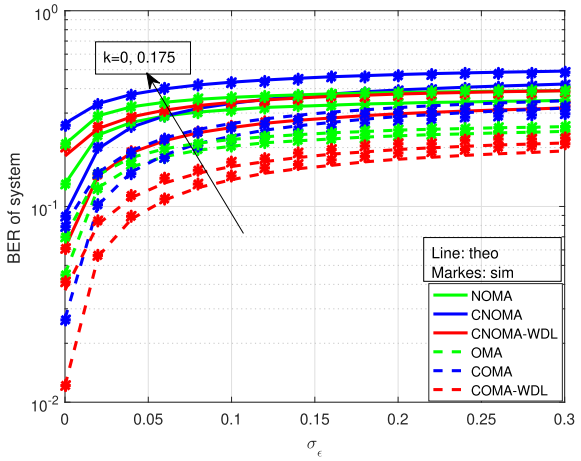

FIGURE 9. BER of system performances of NOMA and OMA w.r.t. σ_ϵ^2, when SNR = 20 dB.

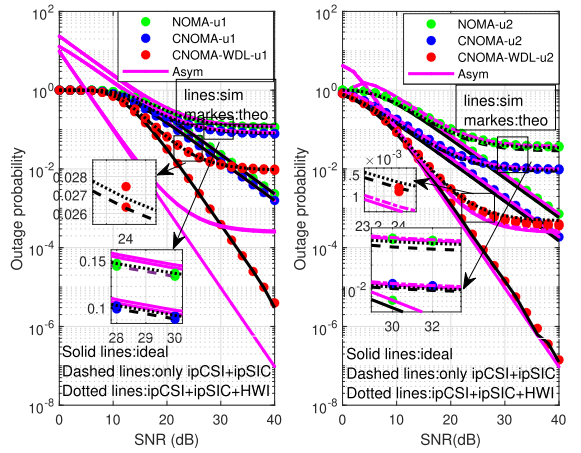

FIGURE 10. OP performances of NOMA, CNOMA and CNOMA-WDL w.r.t. SNR with $\sigma_\epsilon^2 = 0.005$.

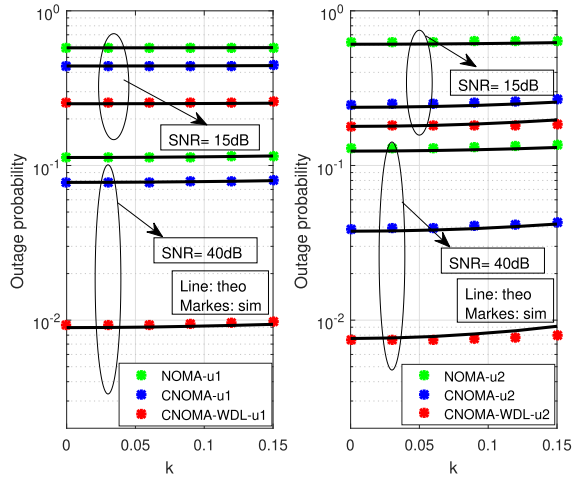

FIGURE 11. OP performances of NOMA, CNOMA and CNOMA-WDL w.r.t. HWI, when $\sigma_\epsilon^2 = 0.005$.

Also, to compare the effect of the channel estimation error on NOMA and OMA schemes, the BER of system performance with SNR= 20 dB is presented in Fig. 9. It is observed that both the NOMA and OMA schemes depend

TABLE 1. Analysis of OP versus HWI coefficient.

			k					
			0	0,03	0,06	0,09	0,12	0,15
NOMA	SNR=15	u1 sim	5.7559 E-1	5.7567 E-1	5.7591 E-1	5.7629 E-1	5.7682 E-1	5.7747 E-1
		u1 theo	5.7555 E-1	5.7562 E-1	5.7585 E-1	5.7622 E-1	5.7674 E-1	5.7741 E-1
		u2 sim	6.0870 E-1	6.0927 E-1	6.1096 E-1	6.1387 E-1	6.1789 E-1	6.2326 E-1
		u2 theo	6.2863 E-1	6.2917 E-1	6.3082 E-1	6.3358 E-1	6.3748 E-1	6.4254 E-1
	SNR= 40	u1 sim	1.1257 E-1	1.1267 E-1	1.1295 E-1	1.1346 E-1	1.1415 E-1	1.1508 E-1
		u1 thep	1.1249 E-1	1.1259 E-1	1.1290 E-1	1.1341 E-1	1.1412 E-1	1.1504 E-1
		u2 sim	1.2417 E-1	1.2439 E-1	1.2521 E-1	1.2654 E-1	1.2842 E-1	1.3104 E-1
		u2 theo	1.2885 E-1	1.2912 E-1	1.2993 E-1	1.3130 E-1	1.3325 E-1	1.3581 E-1
CNOMA	SNR= 15	u1sim	4.3992 E-1	4.3999 E-1	4.4030 E-1	4.4076 E-1	4.4137 E-1	4.4223 E-1
		u1 theo	4.3996 E-1	4.4006 E-1	4.4034 E-1	4.4083 E-1	4.4150 E-1	4.4237 E-1
		u2 sim	2.3850 E-1	2.3926 e-1	2.4137 E-1	2.4507 E-1	2.5054 E-1	2.5790 E-1
		u2 theo	2.4823 E-1	2.4894 E-1	2.5110 E-1	2.5477 E-1	2.6010 E-1	2.6730 E-1
	SNR= 40	u1 sim	7.7402 E-2	7.7469 E-2	7.7706 E-2	7.8100 E-2	7.8644 E-2	7.9319 E-2
		u1 theo	7.7562 E-2	7.7640 E-2	7.7876 E-2	7.8270 E-2	7.8823 E-2	7.9534 E-2
		u2 sim	3.7921 E-2	3.8060 E-2	3.8523 E-2	3.9380 E-2	4.0561 E-2	4.2191 E-2
		u2 theo	3.8955 E-2	3.9111 E-2	3.9584 E-2	4.0393 E-2	4.1571 E-2	4.3172 E-2
CNOMA-WDL	SNR= 15	u1 sim	2.5057 E-1	2.5066 E-1	2.5088 E-1	2.5126 E-1	2.5182 E-1	2.5252 E-1
		u1 theo	2.5476 E-1	2.5486 E-1	2.5517 E-1	2.5567 E-1	2.5638 E-1	2.5729 E-1
		u2 sim	1.7969 E-1	1.8039 E-1	1.8247 E-1	1.8592 E-1	1.9092 E-1	1.9763 E-1
		u2 theo	1.7897 E-1	1.7915 E-1	1.7968 E-1	1.8057 E-1	1.8183 E-1	1.8346 E-1
	SNR= 40	u1 sim	9.028 E-3	9.045 E-3	9.087 E-3	9.164 E-3	9.279 E-3	9.414 E-3
		u1 theo	9.2183 E-3	9.2367 E-3	9.2921 E-3	9.3849 E-3	9.5157 E-3	9.6856 E-3
		u2 sim	7.819 E-3	7.872 E-3	8.052 E-3	8.355 E-3	8.799 E-3	9.418 E-3
		u2 theo	7.4099 E-3	7.4313 E-3	7.4958 E-3	7.6044 E-3	7.7587 E-3	7.9613 E-3

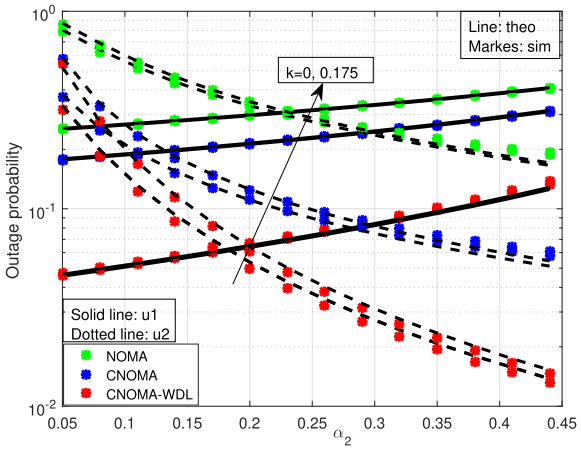

FIGURE 12. OP performances of NOMA, CNOMA and CNOMA-WDL w.r.t. PA, when $\sigma_\epsilon^2 = 0.005$ and SNR = 20 dB.

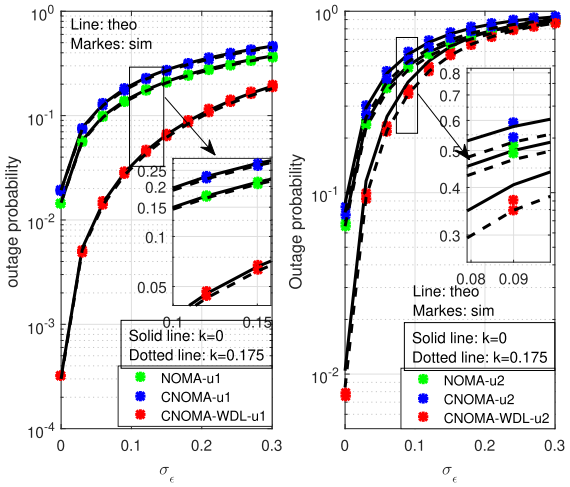

FIGURE 13. OP performances of NOMA, CNOMA and CNOMA-WDL w.r.t. ipCSI with SNR = 20 dB.

on the channel estimation error. The increasing HWI levels degrade the performance of the OMA and NOMA schemes. Again, the OMA is superior to NOMA regardless of the increase in the ipCSI. Thus, regardless of the presence of the HWI and ipCSI, the OMA schemes still perform better than the NOMA schemes. It is clear that the IUI greatly affects the performance of users in NOMA schemes which affects the detection of the users' symbols.

On the other hand, in Fig. 10, we present the OP performance of CNOMA schemes w.r.t. SNR, where the ipCSI is considered as $\sigma_\epsilon^2 = 0.005$, and HWI factor $k = 0.175$. We observe that the asymptotic OP curve is relatively limited over the theoretical curves in high SNR. As we can see that the ipCSI and ipSIC decrease the OP performance. Additionally, the HWI increases the OP performance of both users, it has a lower impact on OP performance compared to ipCSI. The CNOMA-WDL reaches maximal performance than the CNOMA and NOMA.

To evaluate the effect of HWI on the outage performance, in Fig. 11 we present the impact of HWI on the OP performance of the three NOMA schemes. The numerical results

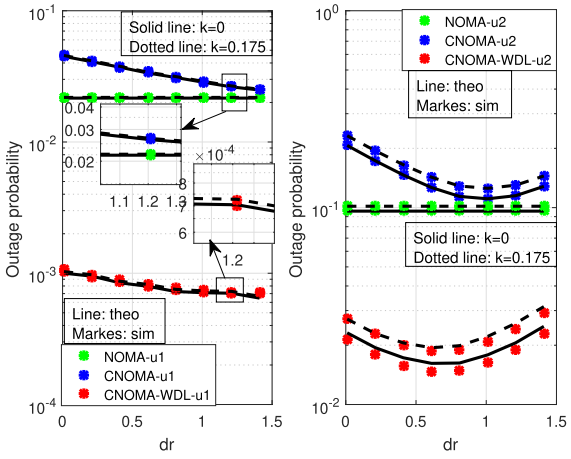

FIGURE 14. OP performances of NOMA, CNOMA and CNOMA-WDL w.r.t. d_r.

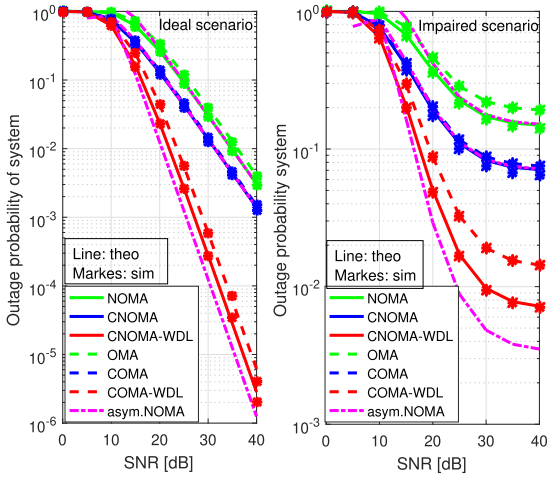

FIGURE 15. OP of system performances of NOMA and OMA, w.r.t. SNR, when $\sigma_\epsilon^2 = 0.005$.

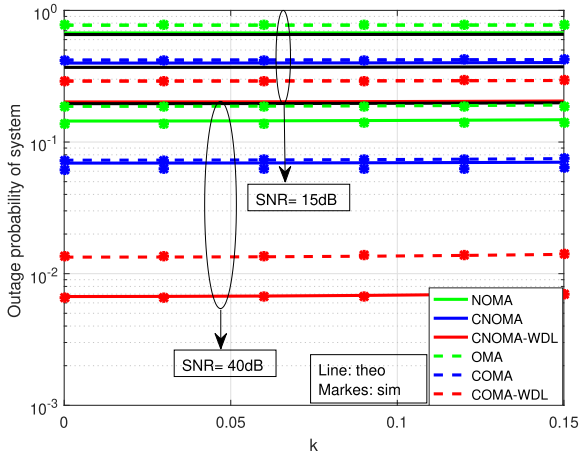

FIGURE 16. OP of system performances of NOMA and OMA w.r.t. HWI level, when $\sigma_\epsilon^2 = 0.005$ and SNR = 15, 40 dB.

are tabulated in Tab.1, which helps us to see clearly the effect of the HWI factor on the performance of the considered system. We observe that the OP performance degrades as the level of HWI increases for the three NOMA schemes. The CNOMA (with/without DL) outperforms the direct NOMA.

In Fig. 12, we present the OP performance versus PA with $\sigma_\epsilon^2 = 0.005$ and SNR = 20 dB, we can observe that increasing PA (α_2), the u2's performance decrease contrary to u1's performance which is improved. With increasing HWI factor, all NOMA's schemes' performances degrade. In particular, the performance of u2 is affected more due to the SIC process.

In order to show the effect of ipCSI, in Fig. 13, we present the OP performance in function ipCSI factor with different HWI values. We can see that the OP performance degrades with the increase of the ipCSI factor. Moreover, compared to ipCSI effects, the HWI has a lower impact on the outage performance.

Fig. 14 presents the OP performance of both users with different R distances. It can be seen that both users achieve better performance when the location of R is nearby the middle. The lower and higher distance between the source and both users means more outage performance in the first and the second phases e.g., when R is near to the source, we will lose the information in the second phase, so more outages occur in the second phase which affects the performance. Likewise, when R is far from the source, we will lose the information from the first phase, causing more outages in the first phase and more outages when the signal is forwarded to the second phase. Thus, in CNOMA, the OP performance of users depends on signal detection in the first and second phases. Also, CNOMA-WDL achieves better performance.

As we have shown in Fig. 14, the users achieve better OP performance when the relay node is nearby the middle. Therefore, to satisfy a fair comparison between the two NOMA and OMA systems. We consider the best relay position to reach the minimum OP performance in both users, so the relay node is considered nearby the middle between the source and users, due to this, we set the distances of the OP of system at $d_{h_{s1}} = 4$m, $d_{h_{s2}} = 2$m, $d_{h_{sr}} = 1.6$m, $d_{h_{r1}} = 2.4$m, $d_{h_{r2}} = 0.4$m.

In Fig.15, we present the OP of system of the NOMA and OMA for different schemes that are obtained in (62), (63) and (64). The asymptotic OP of system for the users of the NOMA with different schemes are also given in (65), (66) and (67). In the high SNR, the asymptotic OP of system curve is limited over the theoretical curves. Besides, we can see that in the ideal or impaired scenario, the OP system of NOMA outperforms OMA for the three schemes.

To compare the effect of HWI on the OP of system, in Fig. 16, we present the OP of system of the NOMA and OMA schemes with $\sigma_\epsilon^2 = 0.005$. We observe that despite the increasing HWI for the two values of SNR (SNR= 15, 40 dB), the NOMA schemes still outperform the OMA schemes.

In Fig. 17, we compare the impact of channel estimation error on the OP of system of the NOMA and OMA schemes with SNR = 20 dB. It can be observed that regardless of the increase of the ipCSI factor, the NOMA schemes are superior to OMA. Thus, regardless of the presence of the

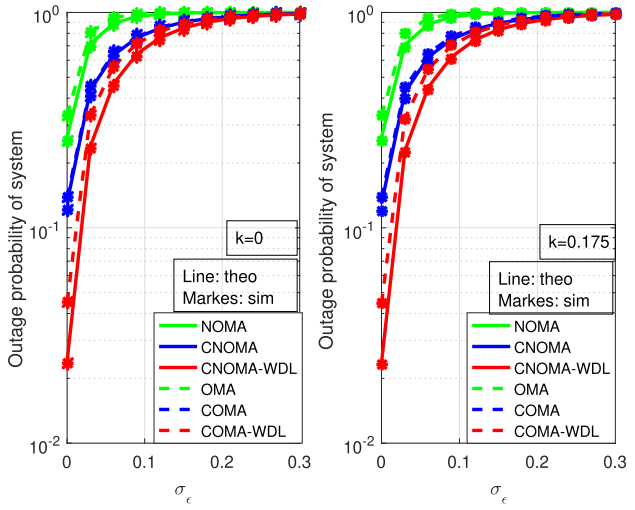

FIGURE 17. OP of system performances of NOMA and OMA w.r.t. σ_ϵ^2, when SNR = 20 dB.

HWI and ipCSI, the NOMA schemes have better performance than the OMA schemes. It can be explained as follows. NOMA has lower time slots than OMA, i.e., NOMA needs a single-time slot for direct links transmission and two-time slots for CNOMA and CNOMA-WDL, while OMA needs two-time slots for the direct links transmission and four-time slots for COMA and COMA-WDL. Because of this, the OP of system of NOMA schemes remains to be superior to OMA schemes despite growing ipCSI and HWI values.

V. CONCLUSION

In this paper, we investigate the BER and OP performance of three NOMA schemes (i.e., downlink NOMA, and cooperative NOMA with and without direct links) under practical assumptions. We consider all imperfections (i.e., ipSIC, ipCSI, HWI) and derive the exact e2e BER and OP expressions for all schemes. All theoretical deductions are validated with computer simulations. We reveal that the BER of NOMA can outperform CNOMA when the HWI is relatively high. The HWI has a lower impact on the OP performance compared to ipCSI on all schemes. Besides, we discuss the effect of PA on the BER and OP performances which present that the PA has an important role; thus, it should be chosen wisely no to cause an error propagation whether from R to users in CNOMA-WDL or an error in SIC processes in all schemes. We believe that this paper can provide fruitful insights for the practical implementation of NOMA schemes and the analysis in this work help researchers to make further analysis for other NOMA schemes under practical assumptions.

APPENDIX. A

The error detection occurs at u1 if the in-phase component of the received signal is less than zero. The error probability for the m_1 symbols at u1 under HWI and ipCSI is given as

$$\begin{aligned} P_{m_1,s1} = \frac{1}{2}\Big(& (P(n+(\sqrt{P_s}(\sqrt{\alpha_1}+\sqrt{\alpha_2})+\eta_{s1})e+\tilde{h}_{s1}\eta_{s1}) \\ & \geq \sqrt{P_s}(\sqrt{\alpha_1}+\sqrt{\alpha_2})\tilde{h}_{s1}) \\ & +((P(n+(\sqrt{P_s}(\sqrt{\alpha_1}-\sqrt{\alpha_2})\eta_{s1})e+\tilde{h}_{s1}\eta_{s1}) \\ \geq & \sqrt{P_s}(\sqrt{\alpha_1}-\sqrt{\alpha_2})\tilde{h}_{s1})\Big). \end{aligned} \tag{68}$$

By using the PDF and Q-function and following all steps in [54], (68) can be expressed as

$$P_{m_1,s1} = \frac{1}{2}\left(\mathrm{Q}(\sqrt{2\delta_{m_1,s1,1}}) + \mathrm{Q}(\sqrt{2\delta_{m_1,s1,2}})\right). \tag{69}$$

The ABER of the u1 is given as

$$\begin{aligned} P_{m_1,s1} = & \frac{1}{2}\int_0^\infty \mathrm{Q}\left(\sqrt{2\delta_{m1,s1,1}}\right) f_{\delta_{m1,s1,1}}(\delta_{m1,s1,1}) d_{\delta_{m1,s1,1}} \\ & + \frac{1}{2}\int_0^\infty \mathrm{Q}\left(\sqrt{2\delta_{m1,s1,2}}\right) f_{\delta_{m1,s1,2}}(\delta_{m1,s1,2})\, d_{\delta_{m1,s1,2}}, \end{aligned} \tag{70}$$

where $f_{\delta_{m1,s1,1}}$ and $f_{\delta_{m1,s1,2}}$ are the is the PDF for the Rayleigh distribution which is defined in [42]. After some algebraic calculations, we find the ABER of u_1 under HWI and ipCSI as given in (18). The proof is completed.

APPENDIX. B

The error to detect m_2 at u2 occurs in two conditions: If m_1 symbols are detected correctly and erroneously. The BER of m_2 at u2 under HWI and ipCSI is given as

$$P_{m_2,s2} = P_{m_2,s2}^{\text{correct}} + P_{m_2,s2}^{\text{error}}, \tag{71}$$

where $P_{m_2,s2}^{\text{correct}}$, $P_{m_2,s2}^{\text{error}}$ are the probability when the m_1 is detected correctly and erroneously at the u2. The probability of error at u2 if m_1 is detected correctly is given as in (72), shown at the bottom of the page. The probability of error at u2 if m_1 is detected erroneously is defined as in (73), shown at the top of the next page. By substituting (72) and (73) into (71) and by using PDF and Q-function, we find BER of u2 to detect m_2 as

$$\begin{aligned} P_{m_2,s2} = \frac{1}{2}\Big(& \mathrm{Q}(\sqrt{2\delta_{m_2,s2,1}}) + \mathrm{Q}(\sqrt{2\delta_{m_2,s2,2}}) \\ & - \mathrm{Q}\left(\sqrt{2\delta_{m_2,s2,3}}\right) + \mathrm{Q}\left(\sqrt{2\delta_{m_2,s2,4}}\right) \\ & + \mathrm{Q}\left(\sqrt{2\delta_{m_2,s2,5}}\right) - \mathrm{Q}\left(\sqrt{2\delta_{m_2,s2,6}}\right)\Big). \end{aligned} \tag{74}$$

$$\begin{aligned} P_{m_2,s2}^{\text{correct}} = \frac{1}{2}\Big(& P(n+(\sqrt{P_s}(\sqrt{\alpha_1}+\sqrt{\alpha_2})+\eta_{s2})e+\tilde{h}_{s2}\eta_{s2} \leq \sqrt{P_s}(\sqrt{\alpha_1}+\sqrt{\alpha_2})\tilde{h}_{s2}) \\ & \times P(n+(\sqrt{P_s}(\sqrt{\alpha_1}+\sqrt{\alpha_2})+\eta_{s2})e+\tilde{h}_{s2}\eta_{s2} \geq \sqrt{P_s}\sqrt{\alpha_2}\tilde{h}_{s2}|n+(\sqrt{P_s}(\sqrt{\alpha_1}+\sqrt{\alpha_2})+\eta_{s2})e+\tilde{h}_{s2}\eta_{s2}) \\ & + P(n+(\sqrt{P_s}(\sqrt{\alpha_1}-\sqrt{\alpha_2})+\eta_{s2})e+\tilde{h}_{s2}\eta_{s2} \leq \sqrt{P_s}(\sqrt{\alpha_1}-\sqrt{\alpha_2})\tilde{h}_{s2}) \\ & \times P(n+(\sqrt{P_s}(\sqrt{\alpha_1}-\sqrt{\alpha_2})+\eta_{s2})e+\tilde{h}_{s2}\eta_{s2} \geq \sqrt{P_s}\sqrt{-\alpha_2}\tilde{h}_{s2}|n+(\sqrt{P_s}(\sqrt{\alpha_1}-\sqrt{\alpha_2})+\eta_{s2})e+\tilde{h}_{s2}\eta_{s2})\Big). \end{aligned} \tag{72}$$

$$
\begin{aligned}
P_{m_2,s2}^{\text{error}} = \frac{1}{2}\Big(&P(n+(\sqrt{P_s}(\sqrt{\alpha_1}+\sqrt{\alpha_2})+\eta_{s2})e+\tilde{h}_l\eta_{s2} \geq \sqrt{P_s}(\sqrt{\alpha_1}+\sqrt{\alpha_2})\tilde{h}_{s2})\\
&\times P(n+(\sqrt{P_s}(\sqrt{\alpha_1}+\sqrt{\alpha_2})+\eta_{s2})e+\tilde{h}_{s2}\eta_{s2} \geq \sqrt{P_s}(2\sqrt{\alpha_1}+\alpha_2)|n+(\sqrt{P_s}(\sqrt{\alpha_1}+\sqrt{\alpha_2})+\eta_{s2})e+\tilde{h}_{s2}\eta_{s2}\\
&\geq \sqrt{P_s}(\sqrt{\alpha_1}+\sqrt{\alpha_2})\tilde{h}_{s2}) + P(n+(\sqrt{P_s}(\sqrt{\alpha_1}-\sqrt{\alpha_2})+\eta_{s2})e+\tilde{h}_{s2}\eta_{s2} \geq \sqrt{P_s}(\sqrt{\alpha_1}-\sqrt{\alpha_2})\tilde{h}_{s2})\\
&\times P(n+(\sqrt{P_s}(\sqrt{\alpha_1}-\sqrt{\alpha_2})+\eta_{s2})e+\tilde{h}_{s2}\eta_{s2} \leq \sqrt{P_s}(2\sqrt{\alpha_1}-\alpha_2)|n+(\sqrt{P_s}(\sqrt{\alpha_1}-\sqrt{\alpha_2})+\eta_{s2})e+\tilde{h}_{s2}\eta_{s2}\\
&\geq \sqrt{P_s}(\sqrt{\alpha_1}-\sqrt{\alpha_2})\tilde{h}_{s2})\Big). \qquad (73)
\end{aligned}
$$

After some algebraic manipulation, we find the ABER of u2 of (74) is as in (22). The proof is completed.

APPENDIX. C

The outage of m_1 at u1 occurs if the received SINR of m_1 is less than the threshold $\gamma_{th,1}$. Hence, by using PDF and CDF as [46, eq. (7) and (8)], the OP of the m_1 at u1 under HWI and ipCSI is computed as

$$
\begin{aligned}
&P_{m1,s1}(out)\\
&= P(\gamma_1^{s1} \geq \gamma_{th,1})\\
&= P(\frac{\alpha_1 P_s|\tilde{h}_{s1}|^2}{\alpha_2 P_s|\tilde{h}_{s1}|^2+\sigma_\epsilon^2 P_s+\sigma_\epsilon^2 P_s k_{s1}^2+|\tilde{h}_{s1}|^2 P_s k_{s1}^2+N_0}\\
&\geq \gamma_{th,1})\\
&= P(|\tilde{h}_{s1}|^2 \geq (\frac{\gamma_{th,1}\left(N_0+\sigma_\epsilon^2 P_s+\sigma_\epsilon^2 P_s k_s 1^2\right)}{\Phi_s 1(\alpha_1 P_s-\gamma_{th,1}P_s\alpha_2-\gamma_{th,1}P_s k_s 1^2)}))\\
&= \int_0^{\frac{\gamma_{th,1}\left(N_0+\sigma_\epsilon^2 P_s+\sigma_\epsilon^2 P_s k_s 1^2\right)}{\Phi_s 1\left(\alpha_1 P_s-\gamma_{th,1}P_s\alpha_2-\gamma_{th,1}P_s k_s 1^2\right)}} \frac{1}{\Phi_s 1}\exp\frac{-y}{\Phi_s 1}\,dy. \qquad (75)
\end{aligned}
$$

Thus, after calculating the integral of (75), we find the OP of m_1 at u1 as given in (41). The proof is completed.

REFERENCES

[1] M. Zeng, W. Hao, O. A. Dobre, and Z. Ding, "Cooperative NOMA: State of the art, key techniques, and open challenges," *IEEE Netw.*, vol. 34, no. 5, pp. 205–211, Sep. 2020.

[2] H. Liu, Z. Ding, K. J. Kim, K. S. Kwak, and H. V. Poor, "Decode-and-forward relaying for cooperative NOMA systems with direct links," *IEEE Trans. Wireless Commun.*, vol. 17, no. 12, pp. 8077–8093, Dec. 2018.

[3] Z. Ding, H. Dai, and H. V. Poor, "Relay selection for cooperative NOMA," *IEEE Wireless Commun. Lett.*, vol. 5, no. 4, pp. 416–419, Aug. 2016.

[4] X. Liang, Y. Wu, D. W. K. Ng, Y. Zuo, S. Jin, and H. Zhu, "Outage performance for cooperative NOMA transmission with an AF relay," *IEEE Commun. Lett.*, vol. 21, no. 11, pp. 2428–2431, Nov. 2017.

[5] D. Wan, M. Wen, F. Ji, Y. Liu, and Y. Huang, "Cooperative NOMA systems with partial channel state information over Nakagami-*m* fading channels," *IEEE Trans. Commun.*, vol. 66, no. 3, pp. 947–958, Mar. 2018.

[6] N. Guo, J. Ge, Q. Bu, and C. Zhang, "Multi-user cooperative non-orthogonal multiple access scheme with hybrid full/half-duplex user-assisted relaying," *IEEE Access*, vol. 7, pp. 39207–39226, 2019.

[7] X. Yue, Y. Liu, S. Kang, A. Nallanathan, and Z. Ding, "Exploiting full/half-duplex user relaying in NOMA systems," *IEEE Trans. Commun.*, vol. 66, no. 2, pp. 560–575, Feb. 2018.

[8] H.-T.-T. Nguyen, T. Nguyen, and X. N. Tran, "Full-duplex cooperative NOMA system under impacts of residual Si and MAI," *Int. J. Electron.*, vol. 108, no. 5, pp. 858–875, May 2021.

[9] V. Aswathi and A. V. Babu, "Full/half duplex cooperative NOMA under imperfect successive interference cancellation and channel state estimation errors," *IEEE Access*, vol. 7, pp. 179961–179984, 2019.

[10] T.-T. T. Nguyen, D.-T. Do, Y.-C. Chen, C. So-In, and M. A. Rahman, "New look on relay selection strategies for full-duplex multiple-relay NOMA over Nakagami-*m* fading channels," *Wireless Netw.*, vol. 27, no. 6, pp. 3827–3843, Aug. 2021.

[11] W. Duan, M. Wen, Z. Xiong, and M. H. Lee, "Two-stage power allocation for dual-hop relaying systems with non-orthogonal multiple access," *IEEE Access*, vol. 5, pp. 2254–2261, 2017.

[12] R. Ramesh and S. Gurugopinath, "Sum rate analysis of cooperative NOMA over dual-hop wireless-power line communication," in *Proc. IEEE 18th India Council Int. Conf. (INDICON)*, Dec. 2021, pp. 1–6.

[13] D. Wan, M. Wen, F. Ji, and R. Huang, "Non-orthogonal multiple access for dual-hop decode-and-forward relay-aided X channel," in *Proc. IEEE 85th Veh. Technol. Conf. (VTC Spring)*, Jun. 2017, pp. 1–5.

[14] Y. Xiao, L. Hao, Z. Ma, Z. Ding, Z. Zhang, and P. Fan, "Forwarding strategy selection in dual-hop NOMA relaying systems," *IEEE Commun. Lett.*, vol. 22, no. 8, pp. 1644–1647, Aug. 2018.

[15] X. Yue, Z. Qin, Y. Liu, X. Dai, and Y. Chen, "Outage performance of a unified non-orthogonal multiple access framework," in *Proc. IEEE Int. Conf. Commun. (ICC)*, May 2018, pp. 1–6.

[16] X. Yue, Y. Liu, Y. Yao, X. Li, R. Liu, and A. Nallanathan, "Secure communications in a unified non-orthogonal multiple access framework," *IEEE Trans. Wireless Commun.*, vol. 19, no. 3, pp. 2163–2178, Mar. 2020.

[17] X. Yue, Z. Qin, Y. Liu, S. Kang, and Y. Chen, "A unified framework for non-orthogonal multiple access," *IEEE Trans. Commun.*, vol. 66, no. 11, pp. 5346–5359, Nov. 2018.

[18] B. Selim, S. Muhaidat, P. C. Sofotasios, B. S. Sharif, T. Stouraitis, G. K. Karagiannidis, and N. Al-Dhahir, "Performance analysis of non-orthogonal multiple access under I/Q imbalance," *IEEE Access*, vol. 6, pp. 18453–18468, 2018.

[19] T. Schenk, *RF Imperfections in High-rate Wireless Systems: Impact and Digital Compensation*. Cham, Switzerland: Springer, 2008.

[20] L. Smaini, *RF Analog Impairments Modeling for Communication Systems Simulation: Application to OFDM-Based Transceivers*. Hoboken, NJ, USA: Wiley, 2012.

[21] T. P. Huynh, T. N. Kieu, T. D. Dinh, M. Voznak, and D. Uhrin, "A performance analysis about impact of I/Q imbalance in AF two-hop relay system," in *Proc. 11th Int. Symp. Telecommun. (BIHTEL)*, Oct. 2016, pp. 1–4.

[22] N. Maletić, M. Čabarkapa, and N. Nešković, "Performance of fixed-gain amplify-and-forward nonlinear relaying with hardware impairments," *Int. J. Commun. Syst.*, vol. 30, no. 6, p. e3102, Apr. 2017.

[23] X. Li, M. Liu, C. Deng, D. Zhang, X.-C. Gao, K. M. Rabie, and R. Kharel, "Joint effects of residual hardware impairments and channel estimation errors on SWIPT assisted cooperative NOMA networks," *IEEE Access*, vol. 7, pp. 135499–135513, 2019.

[24] W. Xie, X. Xia, Y. Xu, K. Xu, and Y. Wang, "Massive MIMO full-duplex relaying with hardware impairments," *J. Commun. Netw.*, vol. 19, no. 4, pp. 351–362, Aug. 2017.

[25] B. C. Nguyen, X. N. Tran, D. T. Tran, X. N. Pham, and L. T. Dung, "Impact of hardware impairments on the outage probability and ergodic capacity of one-way and two-way full-duplex relaying systems," *IEEE Trans. Veh. Technol.*, vol. 69, no. 8, pp. 8555–8567, Aug. 2020.

[26] C. Deng, X. Zhao, D. Zhang, X. Li, J. Li, and C. C. Cavalcante, "Performance analysis of noma-based relaying networks with transceiver hardware impairments," *KSII Trans. Internet Inf. Syst.*, vol. 12, no. 9, pp. 4295–4316, Sep. 2018.

[27] M. Li, B. Selim, S. Muhaidat, P. C. Sofotasios, M. Dianati, P. D. Yoo, J. Liang, and A. Wang, "Effects of residual hardware impairments on secure NOMA-based cooperative systems," *IEEE Access*, vol. 8, pp. 2524–2536, 2020.

[28] C. Deng, M. Liu, X. Li, and Y. Liu, "Hardware impairments aware full-duplex NOMA networks over Rician fading channels," *IEEE Syst. J.*, vol. 15, no. 2, pp. 2515–2518, Jun. 2020.
[29] X. Li, J. Li, and L. Li, "Performance analysis of impaired SWIPT NOMA relaying networks over imperfect Weibull channels," *IEEE Syst. J.*, vol. 14, no. 1, pp. 669–672, Mar. 2020.
[30] X. Li, J. Li, Y. Liu, Z. Ding, and A. Nallanathan, "Residual transceiver hardware impairments on cooperative NOMA networks," *IEEE Trans. Wireless Commun.*, vol. 19, no. 1, pp. 680–695, Jan. 2020.
[31] S. Arzykulov, G. Nauryzbayev, A. Celik, and A. M. Eltawil, "Hardware and interference limited cooperative CR-NOMA networks under imperfect SIC and CSI," *IEEE Open J. Commun. Soc.*, vol. 2, pp. 1473–1485, 2021.
[32] L. Mohjazi, L. Bariah, S. Muhaidat, P. C. Sofotasios, O. Onireti, and M. A. Imran, "Error probability analysis of non-orthogonal multiple access for relaying networks with residual hardware impairments," in *Proc. IEEE 30th Annu. Int. Symp. Pers., Indoor Mobile Radio Commun. (PIMRC)*, Sep. 2019, pp. 1–6.
[33] A. A. Hamza, I. Dayoub, I. Alouani, and A. Amrouche, "On the error rate performance of full-duplex cooperative NOMA in wireless networks," *IEEE Trans. Commun.*, vol. 70, no. 3, pp. 1742–1758, Mar. 2022.
[34] F. Khennoufa, K. Abdellatif, and F. Kara, "Bit error rate and outage probability analysis for multi-hop decode-and-forward relay-aided NOMA with imperfect SIC and imperfect CSI," *AEU-Int. J. Electron. Commun.*, vol. 147, Apr. 2022, Art. no. 154124.
[35] F. Kara and H. Kaya, "Improved user fairness in decode-forward relaying non-orthogonal multiple access schemes with imperfect SIC and CSI," *IEEE Access*, vol. 8, pp. 97540–97556, 2020.
[36] F. Kara and H. Kaya, "Error probability analysis of non-orthogonal multiple access with channel estimation errors," in *Proc. IEEE Int. Black Sea Conf. Commun. Netw. (BlackSeaCom)*, May 2020, pp. 1–5.
[37] T. Assaf, A. Al-Dweik, M. E. Moursi, and H. Zeineldin, "Exact BER performance analysis for downlink NOMA systems over Nakagami-*m* fading channels," *IEEE Access*, vol. 7, pp. 134539–134555, 2019.
[38] H. Yahya, E. Alsusa, and A. Al-Dweik, "Exact BER analysis of NOMA with arbitrary number of users and modulation orders," *IEEE Trans. Commun.*, vol. 69, no. 9, pp. 6330–6344, Sep. 2021.
[39] K. Ferdi and K. Hakan, "A true power allocation constraint for non-orthogonal multiple access with M-QAM signalling," in *Proc. IEEE Microw. Theory Techn. Wireless Commun. (MTTW)*, vol. 1, Oct. 2020, pp. 7–12.
[40] A. Afana, N. Abu-Ali, and S. Ikki, "On the joint impact of hardware and channel imperfections on cognitive spatial modulation MIMO systems: Cramer–Rao bound approach," *IEEE Syst. J.*, vol. 13, no. 2, pp. 1250–1261, Jun. 2018.
[41] F. Kara and H. Kaya, "On the error performance of cooperative-NOMA with statistical CSIT," *IEEE Commun. Lett.*, vol. 23, no. 1, pp. 128–131, Jan. 2019.
[42] M. K. Simon and M.-S. Alouini, *Digital Communications Over Fading Channels*. Hoboken, NJ, USA: Wiley, 2004.
[43] J. G. Proakis and M. Salehi, *Digital Communications*. New York, NY, USA: McGraw-Hill, 2008.
[44] S. M. Ibraheem, W. Bedawy, W. Saad, and M. Shokair, "Full-duplex relaying schemes for cooperative NOMA networks with SWIPT," *Wireless Pers. Commun.*, vol. 124, no. 1, pp. 727–739, May 2022.
[45] X. Huang, F. Yang, X. Liu, H. Zhang, J. Ye, and J. Song, "Subcarrier and power allocations for dimmable enhanced ADO-OFDM with iterative interference cancellation," *IEEE Access*, vol. 7, pp. 28422–28435, 2019.
[46] T. M. C. Chu and H.-J. Zepernick, "Outage probability and secrecy capacity of a non-orthogonal multiple access system," in *Proc. 11th Int. Conf. Signal Process. Commun. Syst. (ICSPCS)*, Dec. 2017, pp. 1–6.
[47] S. Valentin, D. H. Woldegebreal, T. Volkhausen, and H. Karl, "Combining for cooperative WLANs—A reality check based on prototype measurements," in *Proc. IEEE Int. Conf. Commun. Workshops*, Jun. 2009, pp. 1–5.
[48] F. Kara and H. Kaya, "Threshold-based selective cooperative NOMA: Capacity/outage analysis and a joint power allocation-threshold selection optimization," *IEEE Commun. Lett.*, vol. 24, no. 9, pp. 1929–1933, Sep. 2020.
[49] S. Singh and M. Bansal, "Outage analysis of NOMA-based cooperative relay systems with imperfect SIC," *Phys. Commun.*, vol. 43, Dec. 2020, Art. no. 101219.
[50] G. Nauryzbayev, S. Arzykulov, T. A. Tsiftsis, and M. Abdallah, "Performance of cooperative underlay CR-NOMA networks over Nakagami-*m* channels," in *Proc. IEEE Int. Conf. Commun. Workshops*, May 2018, pp. 1–6.
[51] S. Arzykulov, T. A. Tsiftsis, G. Nauryzbayev, and M. Abdallah, "Outage performance of cooperative underlay CR-NOMA with imperfect CSI," *IEEE Commun. Lett.*, vol. 23, no. 1, pp. 176–179, Jan. 2019.
[52] Z. Yang, Z. Ding, P. Fan, and G. K. Karagiannidis, "On the performance of non-orthogonal multiple access systems with partial channel information," *IEEE Trans. Commun.*, vol. 64, no. 2, pp. 654–667, Feb. 2016.
[53] N. T. Tung, P. M. Nam, and P. T. Tin, "Performance evaluation of a two-way relay network with energy harvesting and hardware noises," *Digit. Commun. Netw.*, vol. 7, no. 1, pp. 45–54, Feb. 2021.
[54] F. Kara and H. Kaya, "BER performances of downlink and uplink NOMA in the presence of SIC errors over fading channels," *IET Commun.*, vol. 12, no. 15, pp. 1834–1844, Sep. 2018.

SAFIA BEDDIAF received the B.S. and master's degrees in telecommunication engineering from the University of 8 mai 1945, Guelma, Algeria, in 2014 and 2019, respectively. She is currently pursuing the Ph.D. degree with Echahid Hamma Lakhdar University, El Oued, Algeria. Her research interests include wireless communications networks, non-orthogonal multiple access (NOMA), hardware impairment, IQ imbalance, cooperative communication, and RIS.

ABDELLATIF KHELIL received the B.S. and M.S. degrees in communication engineering from the University of Setif, Algeria, in 2005 and 2009, respectively, and the Ph.D. degree in communication engineering from the University of Setif with the collaboration of UQO University, Canada. Since 2011, he has been with the Department of Electrical Engineering, Echahid Hamma Lakhdar University, El-Oued, Algeria, where he is currently an Associate Professor of communication engineering. He is the author or coauthor of many journals and conference papers. His research interests include wireless communications, cellular communications (5G, B5G, and 6G), MIMO systems, mm-waves propagation, THz communications, new waveforms, and NOMA and RIS.

FAICAL KHENNOUFA received the B.S. and master's degrees in telecommunication engineering from the University of Djillali Liabes, Sidi Bel Abbas, Algeria, in 2012 and 2017, respectively. He is currently pursuing the Ph.D. degree with Echahid Hamma Lakhdar University, El Oued, Algeria. His research interests include wireless communications networks, non-orthogonal multiple access (NOMA), cooperative communication, IQ imbalance, spatial modulation (SM), and energy harvesting.

FERDI KARA (Senior Member, IEEE) received the B.Sc. degree (Hons.) in electronics and communication engineering from Suleyman Demirel University, Türkiye, in 2011, and the M.Sc. and Ph.D. degrees in electrical and electronics engineering from Zonguldak Bulent Ecevit University (ZBEU), Türkiye, in 2015 and 2019, respectively. His Ph.D. thesis is awarded ''Best Ph.D. Thesis'' by IEEE Türkiye Section, in 2021, and Turkish Science Academy (TUBA), in 2022. Since 2011, he has been working with the Wireless Communication Technologies Research Laboratory (WCTLab). He is currently an Assistant Professor with the Department of Computer Engineering, ZBEU, and also a Senior Research Associate with the Department of Systems and Computer Engineering, Carleton University, Ottawa, ON, Canada. He has been listed among World's Top %2 Scientist List by Stanford University and Elsevier, in 2021. His research interests include wireless communications specified with NOMA, MIMO/RIS/LIS systems, cooperative communication, index modulations, energy harvesting, faster than Nyquist signaling, aerial networks, and machine learning algorithms in communications. He has been awarded the 2020 Premium Award for Best Paper in IET Communications and the Best Early Researcher Paper Award in IEEE Blakcseacom2021. He received an Exemplary Reviewer Certificate by IEEE Communications Letters, in 2019, 2020, and 2021. He is also an Editor of IEEE Communications Letters, an Associate Editor of *EURASIP Journal of Wireless Communications and Networking*, and an Area Editor of *Physical Communication* (Elsevier).

HAKAN KAYA received the B.Sc., M.Sc., and Ph.D. degrees in electrical and electronics engineering from Zonguldak Karaelmas University, Türkiye, in 2007, 2010, and 2015, respectively. Since 2015, he has been working as an Assistant Professor with Zonguldak Bulent Ecevit University and the Head of the Wireless Communication Technologies Research Laboratory (WCTLab). His research interests include cooperative communication, NOMA, turbo coding, and machine learning.

XINGWANG LI (Senior Member, IEEE) received the M.Sc. degree from the University of Electronic Science and Technology of China, in 2010, and the Ph.D. degree from the Beijing University of Posts and Telecommunications, in 2015. From 2010 to 2012, he worked as an Engineer at Comba Telecom Ltd., Guangzhou, China. He was a Visiting Scholar at the State Key Laboratory of Networking and Switching Technology, Beijing University of Posts and Telecommunications, from 2016 to 2018. He spent one year as a Visiting Scholar at Queen's University Belfast, Belfast, U.K., from 2017 to 2018. He is currently an Associate Professor with the School of Physics and Electronic Information Engineering, Henan Polytechnic University, Jiaozuo, China. His research interests include MIMO communication, cooperative communication, hardware constrained communication, non-orthogonal multiple access, physical layer security, unmanned aerial vehicles, and the Internet of Things. He has served as a TPC Member for the IEEE GLOBECOM, IEEE WCNC, IEEE VTC, and IEEE ICCC. He has also served as the Co-Chair for the IEEE/IET CSNDSP 2020 of the Green Communications and Networks Track. He also serves as an Editor on the Editorial Board for IEEE Access, *Computer Communications*, *Physical Communication*, *KSII Transactions on Internet and Information Systems*, and *IET Quantum Communication*, and also a Lead Guest Editor for the Special Issue on UAV-enabled B5G/6G networks: Emerging Trends and Challenges of *Physical Communication*, Special Issue on Recent Advances in Physical Layer Technologies for the 5G-Enabled Internet of Things of *Wireless Communications and Mobile Computing*, and Special Issue on Recent Advances in Multiple Access for 5G-enabled IoT of *Security and Communication Networks*.

KHALED RABIE (Senior Member, IEEE) received the M.Sc. and Ph.D. degrees in electrical and electronic engineering from The University of Manchester, in 2011 and 2015, respectively. He is currently a Reader with the Department of Engineering, Manchester Metropolitan University (MMU), U.K. He worked as a part of several largescale industrial projects and has published more than 200 journals and conference papers (mostly IEEE). His current research interest includes designing and developing next-generation wireless communication systems. He is a fellow of the U.K. Higher Education Academy (FHEA). He serves regularly on the Technical Program Committee (TPC) for several major IEEE conferences, such as GLOBECOM, ICC, and VTC. He has received many awards over the past few years in recognition of his research contributions, including the Best Paper Awards at the 2021 IEEE CITS and the 2015 IEEE ISPLC, and IEEE Access Editor of the Month Award, in August 2019. He also serving as an Editor for IEEE Communications Letters and *IEEE Internet of Things Magazine*, an Associate Editor for IEEE Access, and an Executive Editor for the *Transactions on Emerging Telecommunications Technologies* (Wiley). He also guest-edited many special issues in journals, including *IEEE Wireless Communications Magazine*, in 2021, *Electronics*, in 2021, *Sensors*, in 2020, and IEEE Access, in 2019.

HALIM YANIKOMEROGLU (Fellow, IEEE) is currently a Professor with the Department of Systems and Computer Engineering, Carleton University, Canada. He has extensive collaboration with industry resulted in 39 granted patents. He has given over 150 keynotes, tutorials, and invited seminars in the last ten years. His research group has made substantial contributions to 4G/5G wireless technologies. His group's current focus is the wireless infrastructure for the 6G and B6G era with terrestrial, aerial (HAPS and UAV), and satellite network elements. His research interests include wireless communications and networks. He is a member of the IEEE ComSoc Conference Council and the IEEE PIMRC Steering Committee and a fellow of the Engineering Institute of Canada (EIC) and the Canadian Academy of Engineering (CAE). He received several awards for his research, teaching, and service, including the IEEE ComSoc Fred W. Ellersick Prize, in 2021, IEEE VTS Stuart Meyer Memorial Award, in 2020, and IEEE ComSoc Wireless Communications TC Recognition Award, in 2018. He received Best Paper Awards at IEEE ICC 2021 and IEEE WISEE 2021. He is also serving as the Steering Committee Chair for the IEEE Wireless Communications and Networking Conference (WCNC). He served as the general chair and a technical program chair for several IEEE conferences. He has also served in the Editorial Boards for various IEEE Periodicals. He is an IEEE Distinguished Speaker for ComSoc and VTS.